Universität Bielefeld

Grafting Polymers on nanosheets:

A route for the fabrication of freestanding Polymer Brushes

Dissertation

zur

Erlangung des Doktortitels

der Naturwissenschaften

(Dr. rer. nat.)

der Fakultät für Physik der Universität Bielefeld

vorgelegt von

Dipl. Phys.

Ihsan Amin

geboren in Palembang, Indonesien

Bielefeld, Januar 2010

Gutachter: Prof. Dr. Armin Gölzhäuser

Prof. Dr. Rainer Jordan

Hiermit erkläre ich an Eides statt, dass ich die vorliegende Arbeit selbständig und ohne unerlaubte Hilfsmittel durchgeführt habe.

Bielefeld,

Abstract

The fabrication of fully cross-linked and chemically patterned (FCCP) monolayers has been developed in this work. FCCP monolayers can be further chemically functionalized. Chemically defined surface structures are of great practical interest, as they may be used in many technologies such as molecular electronics, biosensors, etc. Crosslinking enhances mechanical stability of FCCP monolayers, so they can be released from the substrate by dissolution from their substrate or by scission of the anchor group-substrate bonds. This results in an extremely flat, two dimensionally extended layer which is better known as a nanosheet. A patterned nanosheet can be transferred either onto a solid substrate such as silicone oxide or silicone nitrate, or to a TEM grid with openings of up to tens of micrometers.

Fabrication of freestanding homogenous and patterned polymer brushes is of great interest for both scientific studies and industrial applications. These materials may find a broad range of applications in many surface-based technologies. We developed a new strategy in preparing freestanding homogenous and patterned polymer brushes: a combination of electron beam chemical lithography (EBCL), 2D carbon-based nanosheet and self-initiated photografting-photopolymerization (SIPGP) to obtain well defined freestanding homogenous and micro- and nanostructured polymer brushes. This new approach offers several advantages:

1. Nanosheets are thermally and mechanically extremely stable. This will make them a good candidate for polymerization at elevated temperatures as well as in intense UV light.
2. EBCL as a patterning tool offers stability, flexibility, selectivity, high throughput and superior resolution.
3. SIPGP offers a simple procedure for preparing polymer brushes. As no SAM modification step is necessary for the preparation of surface-bonded initiator, a tedious, tricky step in the preparation of polymer brushes can be avoided and the polymerization process becomes simplified

With this new approach, a soft and stimuli responsive 10-300 nm thick polymer brush layer is grafted, forming so-called "polymer carpets". These polymer carpets exhibit remarkable properties (optical, wetting) combining extreme thinness, mechanical stability, robustness, flexibility and an unprecedented chemical sensitivity. Precise control of the membrane thickness as well as its mechanical and chemical properties can be obtained by varying the monomer type and polymerization time. Moreover, polymer carpet layers buckle and unbuckle reversibly by applying an external (chemical) stimulus. This unprecedented reversible and fast conformational change is visible by the naked eye and can be applied in the development of new and advanced sensors, displays and micromechanical systems.

Furthermore, freestanding patterned polymer brushes were also successfully fabricated. By combining patterned FCCP nanosheets with subsequent SIPGP, high pattern resolution of freestanding polymer layer, as well as almost-defect free on large area of polymer layer, can be achieved.

Because of their excellent properties, both freestanding homogenous and patterned polymer brushes are very promising for many applications. Freestanding polymer layers will respond faster due to the isolation from the underlying support. This makes them excellent candidates for applications in pressure-based sensors, micro- and nanoactuators, cell adhesion studies and development of microelectromechanical systems (MEMS).

Table of contents

1. Introduction

Surface-based technologies are to a large extent driven by the need for new functional surfaces. Novel methods using both physical and chemical approaches have been introduced in the engineering of designer surfaces and interfaces, spawning opportunities for tailoring surface properties, addressing the needs for numerous application areas, from biomaterials to electronics and many different types of devices.

Self-assembled monolayers (SAMs) have been used intensively as a route to modify and tailor surface chemistry.[1-4] However, a number of limitations of SAMs have now become more apparent. Due to the nature of self-assembling formation, it is practically impossible to obtain defect free large areas. Chemical groups can only be introduced at the surface, whereas in polymer brushes these groups can be carried all along the polymer backbone. Finally, although SAMs can be used to introduce almost any functional group to the surface, it is extremely difficult to introduce reversibly-changing chemical functionalities without reverting to sequential chemical transformations.

To overcome these limitations, polymer brushes grown from SAMs have emerged as an alternative way to provide a route to stable, robust, functional and switchable surfaces.[5-8] Polymer brushes are of particular interest because these surfaces are capable of responding to very subtle changes in the surrounding environment,

such as solvent properties, temperature or light. The grafted polymer chains can extend from the surface into the adjacent liquid phase. Due to the flexibility of the grafted chains, the liquid phase can penetrate the polymer layer and molecules are able to interact with binding partners within the layer. When external stimuli are applied, polymer brushes response by changing their conformational morphology. These reversible switching properties of polymer brushes can be used as both sensing elements and active elements responsive to external stimuli.[5] Polymer brushes have also played an important role in the fabrication of micro- and nanostructured surfaces.[9-10] In the last few years, these surfaces have been the subject of intense research efforts. They have been applied in various fields such as molecular electronics[11], microelectronics, photonics[12-14], microelectromechanical systems (MEMS)[15-16], sensor technology and biology.

While numerous techniques have been developed for the preparation and fabrication of patterned SAMs[10, 17, 18, 19], only a few studies have been dedicated to micro- and nanostructured polymer brushes [20], and even fewer are employed for fabrication of freestanding flexible patterned polymeric grafts. Freestanding polymeric membranes have attracted great attention because they can create permeability and respond faster as a result of their isolation from the supporting substrate. This will be suitable for applications in numerous research fields and applications such as permselective membranes[21], microelectromechanical systems (MEMS) as sensing elements or micro- and nanoactuators[22, 23], displays[24] and nanofluidic and drug delivery systems.

Many strategies have been developed to design freestanding polymeric membranes, such as layer by layer assembly (LBL)[25] and the crosslinking of Langmuir-Blodgett[26]. So far, a common feature of all developed freestanding polymer nanomembranes is the crosslinking of the polymer itself to ensure the mechanical stability of the layer. However, for the fabrication of chemical- or bio-responsive polymer-based nanomembranes, high degree of crosslinking naturally reduces the interaction between the polymer chains and the environment and impairs the sensitivity and flexibility of the films. New strategies need to be developed for the fabrication of these new nanomaterials. Flat, two dimensional cross linked nanosheets fulfill this need. Coming to the scene is electron beam chemical lithography (EBCL) as a powerful tool for patterning because of the selectivity, high throughput and superior resolution that can be achieved.

Freestanding polymer brushes can be prepared by surface-initiated photografting photopolymerization (SIPGP) from a cross linked monolayer (nanosheet). Brushes react faster and have a higher sensitivity towards external stimuli. Hence, soft and stimuli-responsive freestanding polymer brushes could become the system of choice for the development of adaptive layers as actuators and sensors.

The combination of EBCL with nanosheets, that provide excellent properties, and SIPGP which offers a simple route for polymerization, may lead to a new technology platform in the fabrication of both freestanding homogenous and patterned polymer brushes. Grafting polymer brushes on nanosheets and making them freestanding may provide a rich platform on which to exploit and observe nanoscale phenomena and open new perspectives in understanding polymeric systems. This

is an interesting possibility and also a challenging task, where interdisciplinary knowledge in physics, chemistry and biology meet.

2. Research Background

2.1. Grafting Polymers: An Introduction

A polymer brush is defined as an assembly of polymer chains with one end tethered (grafted or anchored) to a surface or interface.[27-29] The brush properties can be controlled by several parameters: grafting density (the number of polymer chains grafted per unit area of substrate), degree of polymerization (DP), chain length and chemical composition of the chains. Polymer brushes can have different chemical compositions (homopolymers, mixed polymers, copolymers, etc.) and molecular architectures (linear, cross-linked, branched, etc.). Depending on grafting density, polymers tethered on a surface can have different physical conformations. When grafting density is low, the segments of individual chains do not 'feel' each other and behave as single, isolated chains tethered to the surface. The thickness of tethered chains, $\boldsymbol{h}$, is independent of $\boldsymbol{\sigma}$, the grafting density of chains on the surface. If the segments of chains weakly adsorb to the underlying surface, the chains form random coils and are linked to the surface by a stem of varying length. Polymer chains maintain a so called "mushroom" conformation with thickness scales as h ~ DP $\boldsymbol{\sigma^0}$ (Fig. 2.1a). If the segments strongly adsorb to the underlying surface, the polymer chains obtain a flat, "pancake" like conforma-

tion (Fig. 2.1b). At high grafting density, the situation is completely different. Polymer molecules become densely packed and start overlapping. The segments of the chains become crowded. However, the chains will try to avoid overlapping as much as possible and minimize the strong segment-segment interaction by changing from coil to a stretching-away ("brush"-like) conformation perpendicular to the surface (Fig. 2 1c) with the thickness given by h ~ DP $\boldsymbol{\sigma}^{1/3}$

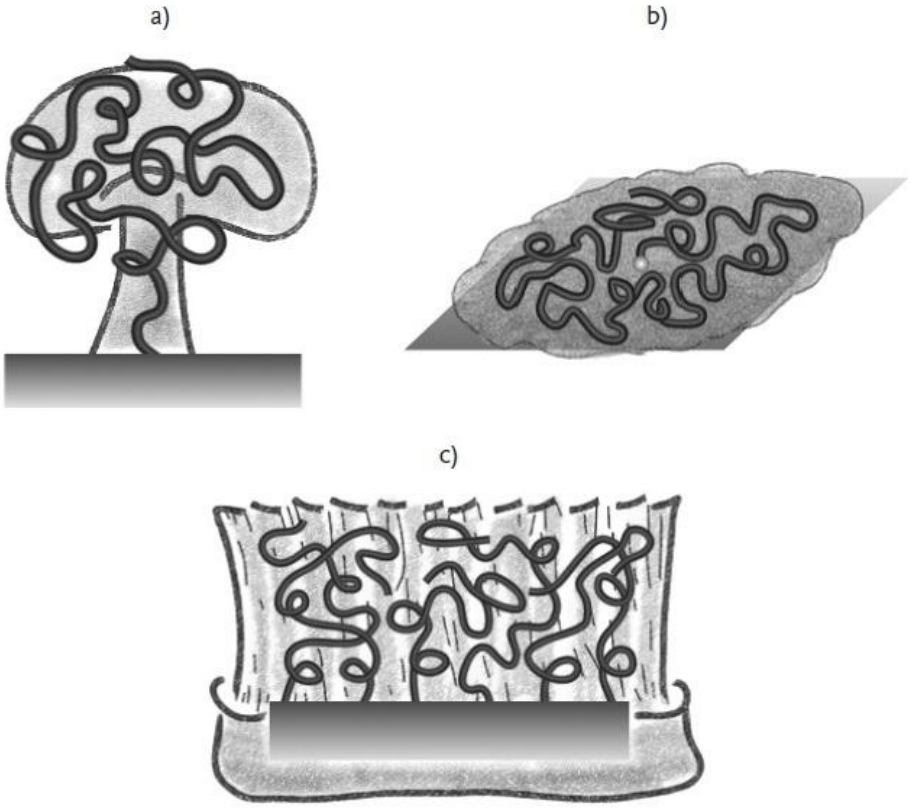

Figure 2.1 Artistic impression of three different physical conformations of polymers tethered on a surface: a) "mushroom", b) "pancake", and c) brush conformation (from ref. [8]).

The stretched-away polymer chains have molecular conformations different from free, flexible polymer chains in solution where chains adopt a 'random-walk' configuration. Due to the stretching of the chains which are perpendicular to the surface, several new physical phenomena arise, for example autophobicity, in which chemically identical free polymer chains do not wet their own brushes.[30-31]

Solvents can be either present or absent in polymer brushes. In a good solvent, sometimes referred to as the wet state, polymer chains swell to maximize contact with solvent molecules by avoiding each other and adopt an expanded coil or stretched conformation. The interaction between polymer chains and solvent molecules is favorable and the loss of entropy during the chain stretching process is compensated for by the establishment of a chemical bond that connects the polymer to the surface. In this condition, the radius of gyration of a polymer, a measure of the macromolecular size, is given by $R_g \sim DP^{3/5}$. In a bad solvent, polymer chains collapse to minimize contact between polymer and solvent molecules, giving the radius of gyration of polymer, $R_g \sim DP^{1/3}$ [32]. In dry conditions, the polymer chains collapse: this state is referred to as the collapsed chain conformation. Steenackers et al. reported that the thickness of a polymer layer in the collapsed state (dry thickness $\boldsymbol{h_d}$) is given by [33]:

$$h_d = \frac{M_n \, \sigma}{\rho \, N_{AV}} \qquad \text{(Eq. 1)}$$

M_n, σ, ρ, and N_{AV} are the number-average molar mass, grafting density, bulk density of grafted polymer and Avogadro's number, respectively.

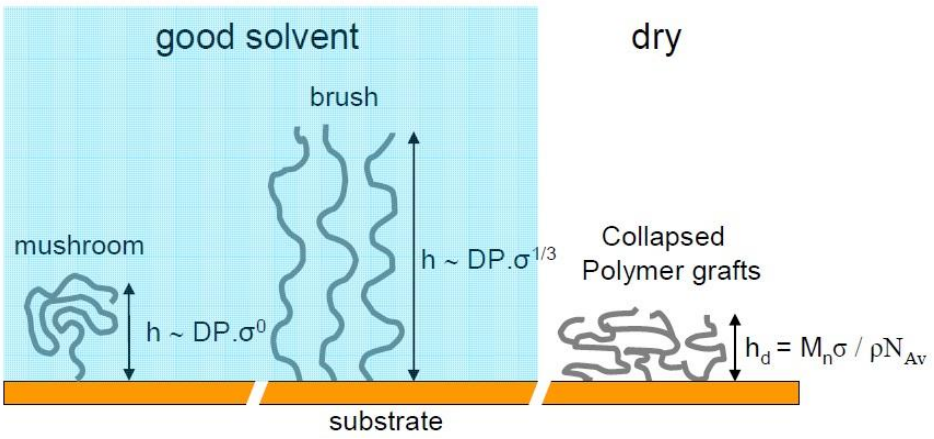

Figure 2.2. In the presence and absence of solvent, different physical conformations of polymer chains tethered on surface are obtained: mushroom (left), brush-like (middle) and collapsed conformation (right). From ref. [20].

2.2. Synthesis of Polymer Brushes

Polymer brushes on solid surfaces can be prepared by using *grafting to* and *grafting from* methods. In the *grafting to* approach, preformed, end-functionalized polymer chains react with an appropriate surface or interface. Although the *grafting to* approach is experimentally very easy to perform, it has one intrinsic problem: during the process of surface attachment, the end-functionalized, reactive chains on polymers will compete with already attached chains on the surface. With an increasing polymer coverage, the already attached chains form a kinetic barrier which restricts the attachment of further chains to the surface, resulting in low

grafting density (the number of anchored polymer chains per surface area), and thus, a low film thickness. Polymer films generated by this method are limited to between 1 – 5 nm thickness.[8]

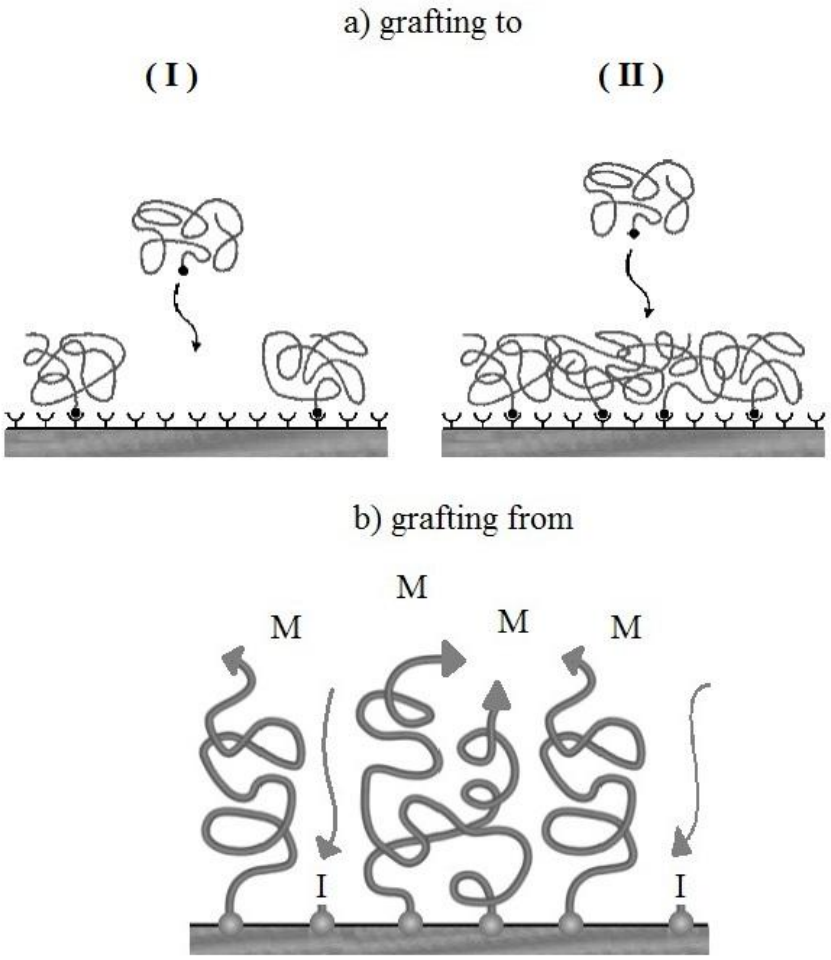

Figure 2.3. Schematic illustration of grafting to and *grafting from* process. In the grafting to process, macromolecule polymers are readily attached to a surface (a.I). As the coverage increased, the already attached polymer chains prevent further attachment of polymer chains (a.II). In the grafting from process, small monomer molecules (M) are grown from initiators (I) bound to the surface.

In the *grafting from* approach, a surface with immobilized initiators is prepared, followed by surface initiated polymerization to generate tethered polymers. In other words, polymer chains are grown from the initiators bound to a surface. For this reason, the *grafting from* approach is also called surface initiated polymerization (SIP). Unlike in the *grafting to* method, where macromolecule polymers are grafted directly to a surface, in the *grafting from* method, the active-end initiator chains are easily accessible for monomer units. Thus, a high grafting density is reached and a thick polymer layer is obtained.

2.3. Surface initiated polymerization

In SIP, immobilization of initiators on a surface plays a vital role in polymer synthesis. There are many strategies to bind initiators on a surface. The most common strategy is immobilization of initiators on well-defined self-assembled monolayers (SAMs). Alkylsilane[34] and alkanethiol SAMs[35] are the most commonly used SAMs for providing reliable initiators for SIP (a more detailed discussion on SAMs can be found in literature[1-3]). With this method, a high density of initiators on the surface is achieved, which leads to a well-defined initiation mechanism. For this reason, this technique has become the most widely preferred. Azo- and peroxide compounds are typical initiators used for polymerization reactions.[36]

These compounds act as bifunctional molecules with an initiator function at one end and a surface grafting function at the other end. Another strategy for immobilization of initiators on a surface or substrate is treating the substrate directly with plasma or glow-discharge. This treatment leads to the formation of initiator moieties on the surface, which can be used for polymerizations. This SAM-free technique has drawn attention recently. Fukuda et al.[37], reported on the formation of a sufficient amount of peroxides as initiating moieties by O_2-plasma treatment. Kang et al.[38] have used radio frequency Ar plasma pretreatment, followed by air exposure to generate peroxide initiators. Many reports on SAM-free technique can be found in literature.[37-42]

Since the seminal work of Prucker and Rühe[43, 44], SIP techniques, such as living ring opening, living cationic[45], living anionic[46], ring opening metathesis polymerization (ROMP)[47], and free radical polymerization[43, 44, 48], have been widely used to produce polymer brushes. Difficulties in controlling the propagation and termination of the polymerization reaction usually result in low homogeneity in chain length. To overcome this problem, living radical polymerization techniques such as nitroxide mediated polymerization (NMP)[49], atomic transfer radical polymerization (ATRP)[50-51], reverse ATRP[52-53] and reversible addition-fragmentation chain transfer (RAFT)[38, 54], have been widely used and become more popular as they can be used with a wide range of monomers. In general, it can be said that SIP has attracted enormous attention over the past decade for providing simple and robust synthetic routes to well-defined, polymer layers.

Progress in synthesis techniques makes it possible to obtain polymer chains with controlled length and morphology.

2.4. Self-initiated photografting and photopolymerization

In the previous section, we have discussed how polymer layers are synthesized by using the most common technique, surface initiated polymerization. As mentioned before, in SIP a surface pretreatment is required with initiator compounds or methods leading to the formation of initiator moieties. The functionalization step to introduce suitable initiators for SIP can be tedious for wider applications. Ranby et al. reported a bulk surface photografting photopolymerization procedure.[55] Their technique allows formation of polymer brushes without pre-immobilization of initiators on the surface; they have successfully grafted very dense and thick (2 – 5 μm) polymer layers directly onto cross-linked polymer substrates such as polyethylene, poly(ethylene terephthalate) and nylon. The procedure is very simple and fast: a substrate is immersed in bulk monomer solution in which a small amount of benzophenone (BP) is added as photoinitiator. This is followed by exposure to UV light with a spectral distribution of 300 - 400 nm. The photoinitiator should be a compound that is thermally stable, and capable of absorbing light (photoexcitation) and transfer its energy to another molecule.

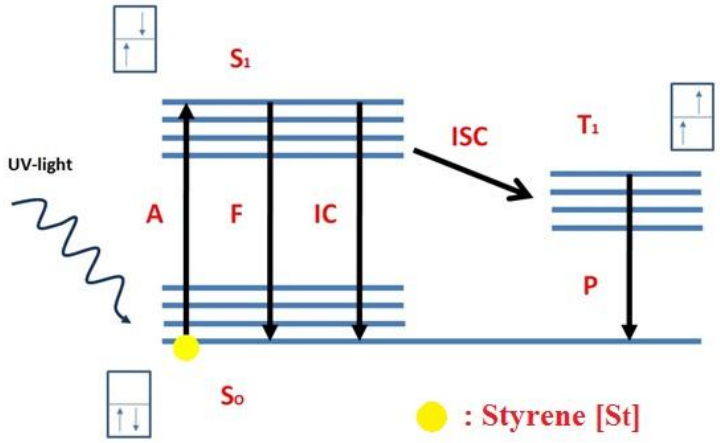

Figure 2.4 The energy diagram of a possible mechanism in bulk photografting of styrene [St] (ref. 55-56). S_O is the ground state, and S_1 is the lowest excited singlet state, T_1 is the lowest triplet state A is absorption, F is Fluorescence, IC is internal conversion, ISC is intersystem crossing and P is phosphorescence.

Further study by the same authors showed that BP played only a small role in the polymerization process; in the total absence of BP, polymer brushes (styrene) were obtained with the same grafting efficiency on a PE substrate.[56] Thus, by simply immersing a substrate into bulk monomer, and by irradiation with UV-light, polymer brushes can be grafted directly to the surface. To explain how this could happen, Li et al. proposed the most likely mechanism[57]: when irradiated with UV light, styrene will absorb photon energy and acts as photoinitiator. It will be excited to the higher singlet state $[St]^{S1}$ and can be transformed into a more stable triplet state containing two free radicals $[\cdot St\cdot]^{T1}$ via ISC. $[\cdot St\cdot]$ can initiate a free radical polymerization in solution and at the same time abstract a hydrogen atom from the PE substrate, leading to the formation of radicals on the surface which further initiates the free-radical surface initiated polymerization of styrene.

They named this mechanism *self-initiated photografting and photopolymerization* (SIPGP). More results on photografting were reported elsewhere.[58, 59, 60, 61] Similar results on photografting of various acrylic monomers on high density PE substrates were reported by Brown et al.[58]: similar to styrene, acrylic monomers can also absorb UV-light and be excited to a higher excited state with enough energy to abstract hydrogen from the surface and initiate polymerization. Monomers which have been successfully grafted on PE substrates are shown in fig.2.5.[57, 58]

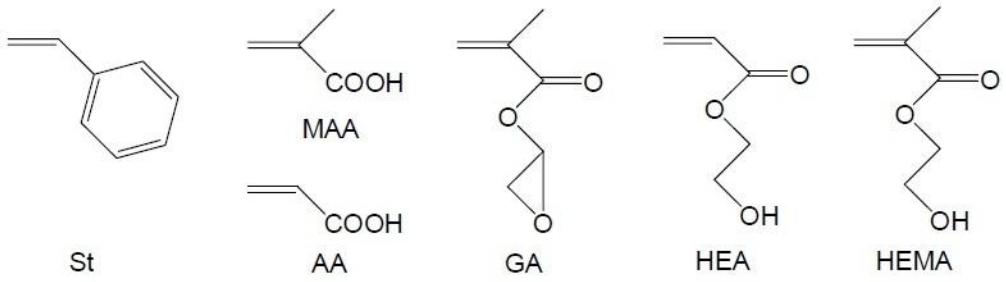

Figure 2.5. Monomers that have been successfully grafted on PE substrates are: styrene (St), acrylic acid (AA), methacrylic acid (MAA), glycidyl acrylate (GA), 2-hydroxyethyl acrylate (HEA), and 2-hydroxyethyl methacrylate (HEMA).

Dyer et al. were the first to perform SIPGP on SAMs.[62] They reported on the formation of approximately 200 nm PS and 675 nm PMMA brushes on gold containing tertiary amines. The SAMs were immersed directly into a monomer solution and irradiated with UV-light. They suggest that the photoactivated monomer activates the amino group by electron transfer or hydrogen abstraction.

SIPGP provides a simple procedure for preparing very thick and dense polymer layers. Furthermore, the handling of a UV-sensitive system is very easy and special precautions such as safety light conditions, which are mandatory for a visible

light system, are not required. However, despite the advantages it offers, SIPGP has not attracted much attention in the polymer synthesis community.

2.5. Patterning polymer brushes

Patterned polymer brush nano- and microstructures have gained evermore attention over the past few years, because of their ability to modify surface properties and their potential for a broader range of applications in surface-based technologies.[63-66] By patterning polymer brushes, control is achieved over functionality, feature dimension and shape. Fabricating patterned brushes with defined properties is very important for a wide range of research studies and applications such as biosensors[67, 68], microelectronics[69], for particle capture and release in micro- and nanofluidic devices[70-73], proteomic chips[74] and bio-related and medicinal research, including usage of polymer brushes as substrates for bone cells[75], protein immobilization[76], cell adhesions and tissue engineering.[77-79] Various strategies for obtaining patterned polymer brushes have been demonstrated by many research groups, such as photolithography[80], electron beam chemical lithography[81-83], scanning probe based lithography (nanoshaving, nanografting and dip-pen lithography)[84-87] and microcontact printing (μCP)[70, 88-89]. These methods rely on the *grafting from* approach (SIP) where polymer brushes are grown from predefined, functionalized, patterned SAMs. The combination of patterned SAMs

and subsequent SIP allow a superior control over the growth of patterned polymer brushes. Detailed discussions on various lithographic methods can be found in literature.[70-89] Here we focus on electron beam chemical lithography (EBCL).

2.5.1. Electron beam chemical lithography

Electron beam lithography (EBL) utilizes a focused electron beam scanning across a surface covered with a resist film sensitive to those electrons, thus depositing energy in the desired pattern in the resist film. Derived from an early generation of the scanning electron microscope (SEM)[90], EBL has become the most developed technique in nanofabrication and is widely used for pattern fabrication. While smaller patterns in the nanometer range can be achieved by focused electron beam, larger pattern areas can be obtained by proximity printing, using an electron flood gun combined with a stencil mask. Gölzhäuser et al. have been developing and utilizing the electron-induced patterning of biphenyl SAMs in great detail.[91-95] In their early work, they reported that C-H cleavage occurs upon irradiation of 1, 1'-biphenyl-4-thiol (BPT) with 50eV electrons, followed by crosslinking between neighboring phenyl units. During this process, the crosslinked molecules maintain their preferred orientation and only a little material desorbs. Hence, the electrons generate a well ordered and cross-linked monolayer (Fig. 2.6a). They also demonstrated that the cross linked monolayer is chemically stable and has an

increased wet-etching resistance against KOH/KCN.[91] Later on, they demonstrated the fabrication of a free-standing nanosheet of crosslinked biphenyl SAMs which is mechanically extremely stable.[96] When 4'-Nitro-1, 1'-biphenyl-4-thiol (NBPT) SAMs are used, the hydrogen atoms liberated from the aromatic cores by electron irradiation, locally reduce the nitro to an amino group (Fig. 2.6b). This process results in cross linked 4'-Amino-1,1'-biphenyl-4-thiol (cABPT) where the amino groups can be chemically modified further.[92]

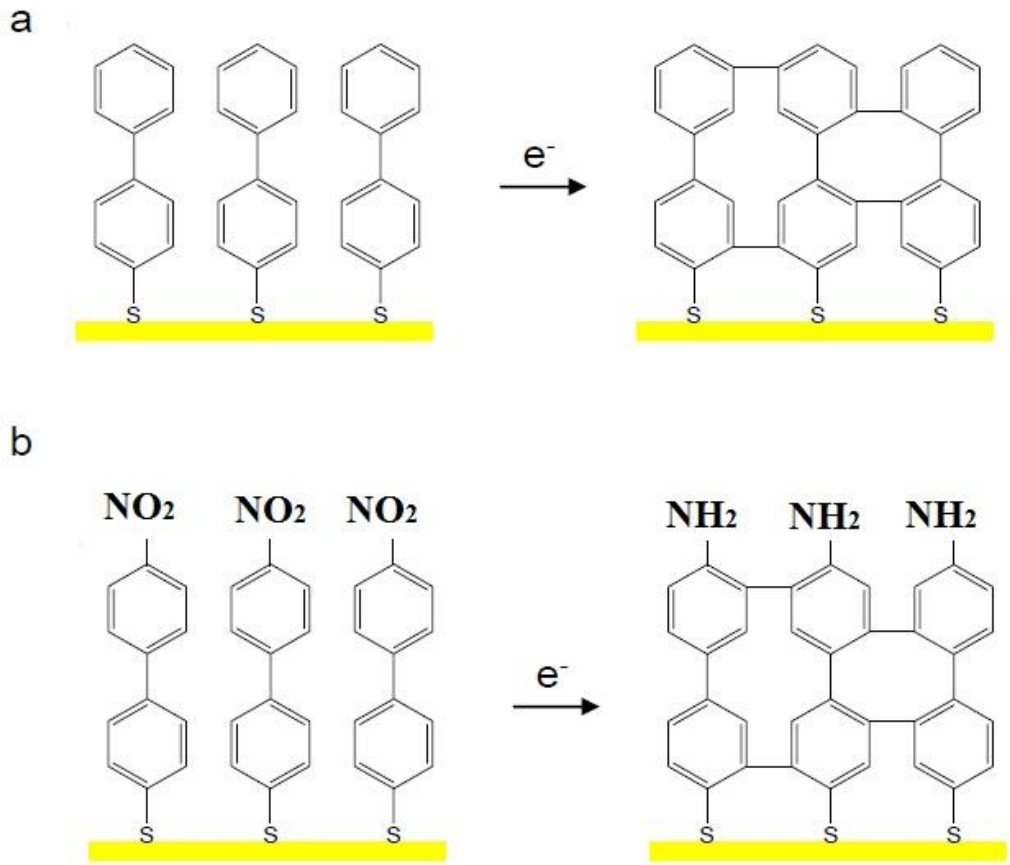

Figure 2.6. Scheme of electron induced crosslinking process in aromatic SAMs (a) BPT and (b) NBPT SAMs (from ref. 91-93).

The electron beam induced conversion of one chemical function to another (here: nitro to amino) is called electron beam chemical lithography (EBCL). Modification and fabrication of defined chemical nanostructures becomes possible. Schmelmer et al. reported on the preparation of patterned polystyrene (PS) brushes by combining EBCL of NBPT SAMs and amplification of the primary structure by SIP of styrene, as schematically shown in fig. 2.7.[83]

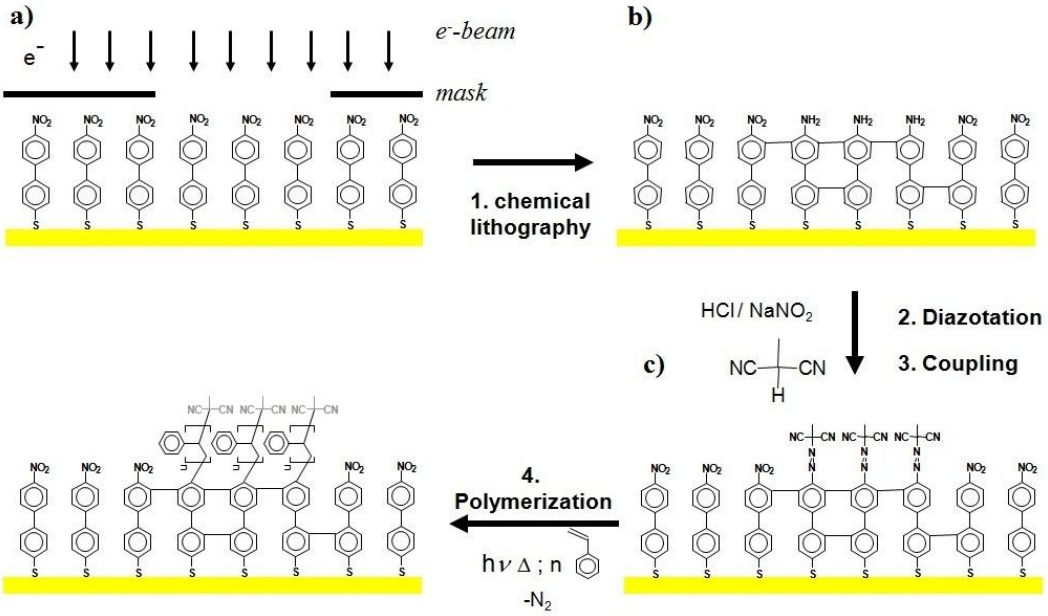

Figure 2.7 Schematic procedure of SIP patterned polystyrene brushes. NBPT SAMs is exposed to an electron beam, generating patterns with terminal amino groups (1). Next, diazotization and coupling with malonodinitrile gives a SAM bearing an asymmetric azo initiator, cAMBPT (2-3). Finally, exposure to a vinyl monomer (styrene) and heating at 80 °C, radical polymerization occurs, resulting in a polymer brush layer (from ref. 83).

Irradiation of NBPT SAMs was performed through a stencil mask with circular openings of 1.6 µm which generated initial patterns with amino functional groups. The terminal amino groups were then diazotized and treated with methylmalono-

dinitrile to give a surface-bound monolayer bearing an azo-initiator, (4'-azomethylmalonodinitrile-1, 1'biphenyl-4-thiol, cAMBPT). Phenyldiazenyl-alkylmalonodinitriles and their derivatives are suitable initiators for radical polymerization of a large variety of vinyl compounds in solution[97], as well as SIP[98, 99]; Azoinitiators such N, N-azobisisobutyronitril (AIBN) are commonly used for radical polymerization. AIBN can be thermally or photochemically activated. This means that an AIBN-modified surface can undergo photopolymerization. It has been reported that surface-initiated photopolymerization (SIPP) of styrene at room temperature leads to denser, more homogenous, and significantly thicker layers when compared to thermally initiated SIP. The cAMBPT monolayer was then exposed to styrene and heated to 80 ℃. Radical polymerization started and resulted in polystyrene brushes in irradiated patterned (Fig. 2.8a). AFM measurement on the structured polystyrene brushes revealed a typical height of 6 nm on PS spots, as shown in Fig 2.8b.

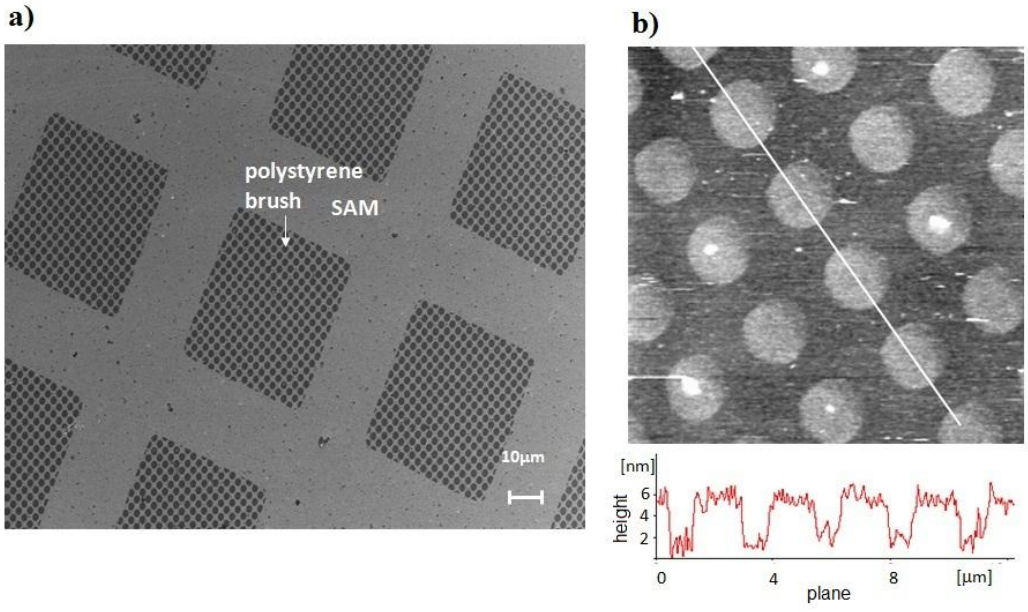

Figure 2.8. Structured polystyrene dots obtained by a combination of EBCL of NBPT SAMs followed by a SIP process in patterns. a) SEM image of polystyrene spots. The dark dots represent patterned areas where NBPT was converted into cABPT, treated further to form cAMBPT, and where SIP of styrene takes place. b) AFM image of small area of the same substrate, showing polystyrene spots of 6 nm thick (from ref. 83).

The electron induced crosslinking of biphenyls enhances the stability of the monolayer and allows the polymerization at elevated temperatures or with intense UV light. This result reflects the capability of a one-to-one translation of the original mask to the surface at high resolution of patterned polymer brushes, indicating that by using EBCL, enhanced stability, significant selectivity and uniformity of the process on a large scale can be achieved.

In recent years, Steenackers et al. have used SIPGP for preparation of structured polymer grafts on surfaces.[100]

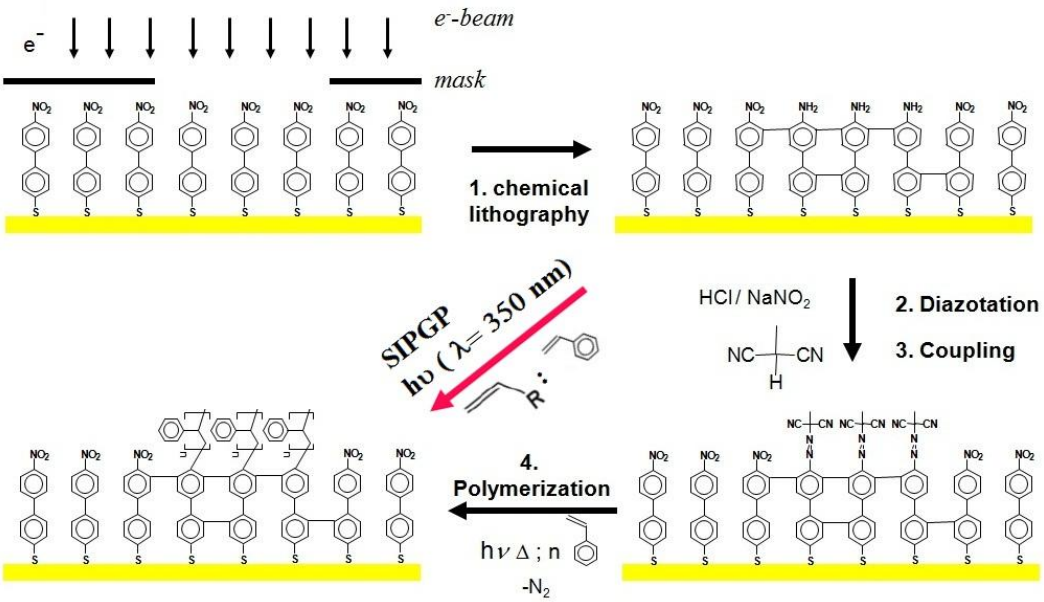

Figure 2.9. Preparation of structured polymer brushes by SIPGP.

Their results show that highly defined structured polymer brushes can be prepared by the SIPGP of styrene and acrylic monomers directly onto biphenylthiol SAMs on gold, patterned by EBCL, as schematically shown in Fig. 2.9. This renders the SAM-modification step for the preparation of surface-bonded initiator unneces-

sary. Thus, a tedious, tricky step in preparation of polymer brushes can be avoided and the polymerization process is simplified.

The stability, selectivity, high throughput and superior resolution of patterned, functionalized SAMs offered by EBCL combined with SIPGP make it an ideal technology platform for the preparation of structured polymer brushes.

2.6. 2D carbon nanosheets

When aromatic SAM is irradiated with electrons, the electrons generate a well ordered and crosslinked monolayer. Crosslinking enhances the stability of a monolayer. Cross linked SAMs can be released from the substrate by dissolution of the substrate or by scission of the anchor group-substrate bonds, resulting in an extremely flat, two dimensionally extended layer which is better known as a nanosheet. Gölzhäuser et al. have developed the fabrication of carbon-based biphenyl nanosheet very far. In their preliminary work, they reported on the preparation of freestanding biphenyl nanosheet with the thickness of a single molecule.[96, 101] These carbon nanosheets can span holes ranging in a size up to several tens of micrometers. These authors also reported the fabrication of circular-shaped nanosheets. The circular shape was obtained by pre-patterning the biphenyl SAM

by using EBCL when a mask with circular holes was placed on the SAM substrate. Thus, patterned nanosheet can be fabricated.

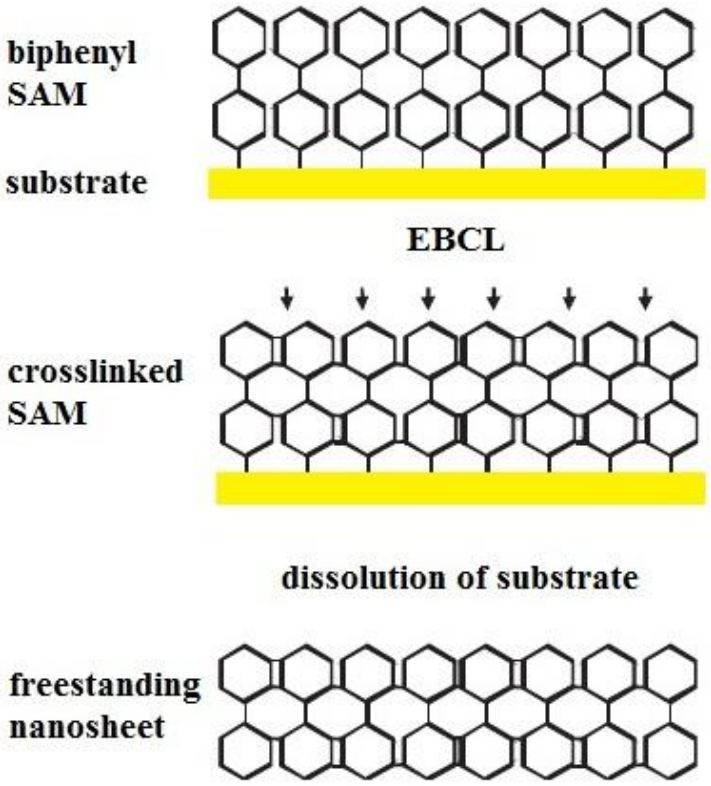

Figure 2.10. Preparation of freestanding nanosheet.

Their recent work shows that a biphenyl nanosheet is extremely stable both thermally and mechanically.[102] A thermally stable nanosheet will resist intense UV light. This provides an ideal surface for photopolymerization. The combination of nanosheets with excellent properties and SIPGP leads to a new strategy in fabricating both freestanding homogenous and patterned polymer brushes.

3. Research Objectives

The purposes of this work were to fabricate and study freestanding homogenous polymer brushes grafted on nanosheet as well as freestanding patterned polymer brushes.

Fabrication of freestanding homogenous and patterned polymer brushes is of a great interest for both scientific studies and industrial applications. These materials may find a broad range of applications in many surface-based technologies. We developed a new strategy in preparing freestanding homogenous and patterned polymer brushes: a combination of electron beam chemical lithography (EBCL), 2D carbon-based nanosheet and self-initiated photografting photopolymerization (SIPGP) to obtain well defined freestanding homogenous and micro- and nanostructured polymer brushes.

This new approach offers several advantages:

1. A Nanosheet is extremely thermally and mechanically stable. This will make it a good candidate for polymerization at elevated temperature as well as intense UV light.
2. EBCL as a patterning tool offers stability, flexibility, selectivity, high throughput and superior resolution.
3. SIPGP technique offers a simple procedure in preparing polymer brushes. As a SAM-modification step is no longer necessary for the preparation of surface-bonded initiator, a tedious, tricky step in the preparation of poly-

mer brushes can be avoided and the polymerization process becomes simplified.

What does the morphology of the polymer brushes grafted on nanosheets look like? How will these brushes respond to external stimuli? And how do nanostructured polymer grafts behave in various conditions? Will new phenomena emerge? What will be possible applications? Further work could concentrate on the development of this new strategy and may open new perspectives in understanding 2D polymeric system.

4. Experimental Part

4.1. Sample preparation

4.1.1. Preparation of biphenylthiol SAMs on gold

1,1'-biphenyl-4-thiol (BPT) and 4'-Nitro-1,1'-biphenyl-4-thiol (NBPT) were prepared on gold substrates. First, mica substrates with a layer of 300 nm thermally evaporated Au were cleaned in a UV/ozone-cleaner (UVOH 150 LAB from FHR, Germany) for 3 minutes, rinsed with ethanol and blown dry in a stream of nitrogen. They were then immersed in a 10 mM solution of 4'-nitro-1,1-biphenyl-4-thiol (NBPT, purchased from Taros Chemicals) or 1,1-biphenyl-4-thiol (BPT, purchased from Platte Valley Scientific) in N,N-dimethylformamide (DMF p.a., purchased from VWR, dried with 0.4 nm molecular sieve) at room temperature for 3 days. Subsequently the samples were rinsed with DMF and ethanol (p.a., purchased from VWR) and finally dried in a stream of nitrogen.

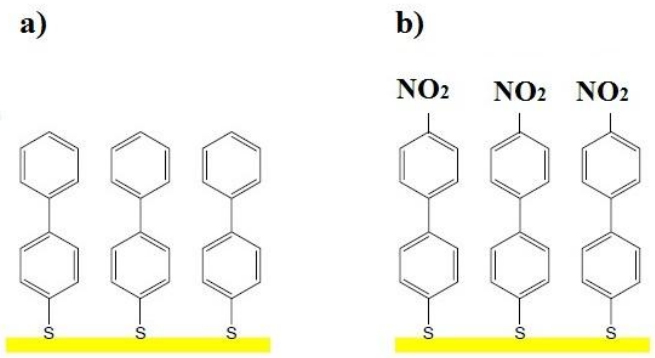

Figure 4.1. shows cartoon of a) BPT and b) NBPT SAMs.

4.1.2. Patterning of biphenylthiol SAMs by chemical lithography

Cross-linking was achieved in high vacuum (<5 x 10^{-7} mbar) with an electron flood gun (Specs FG20) at an electron energy of 100 eV and typical dose of 50 mC/cm^2 for homogeneous SAMs. The dose was measured with a Faraday cup in close proximity to the sample. For chemically patterning, a carbon quantifoil is used as shadow mask and placed on the sample during irradiation.

4.1.3. Preparation of Nanosheets.

The cross-linked SAMs were transferred from the mica substrates to silicon substrates with either a 300 nm thick oxide layer or a 150 nm thick silicon nitride layer on top of a 10 nm oxide layer. This transfer was achieved by cleaving the cross-linked SAM from its substrate using a layer of PMMA for stabilization. A ~400 nm thick layer of PMMA was spincoated onto the sample and baked on a hotplate. The Au was cleaved from the mica by immersion in hydrofluoric acid (48%) for 5 min and etched away in an I_2/KI-etch bath (~15 min). Afterwards the nanosheet/PMMA was transferred onto SiO_2 or Si_3N_4 substrate followed by dissolution of the PMMA in acetone, rinsing the sample with methanol and drying in a stream of nitrogen. SiO_2/Si_3N_4 substrates were always cleaned with piranha (H_2SO_4:H_2O_2 = 3:1) solution before use.

4.1.4 Self-Initiated Photografting and Photopolymerization (SIPGP).

The silicon supported nanosheets were submerged in about 1 mL of freshly distilled and degassed styrene, methyl methacrylate (MMA) or 4-vinylpyridine (4VP) (Fluka) in a glass photoreaction vial. Polymerization was performed under an argon atmosphere for different time periods under irradiation with UV-light (λ_{max} = 350 nm) at room temperature. After polymerization, the samples were removed from the reaction solution and immediately washed with a good solvent for the respective polymer (PS in toluene; PMMA in acetone; P4VP in ethanol). The samples were additionally cleaned in ethyl acetate and ethanol.

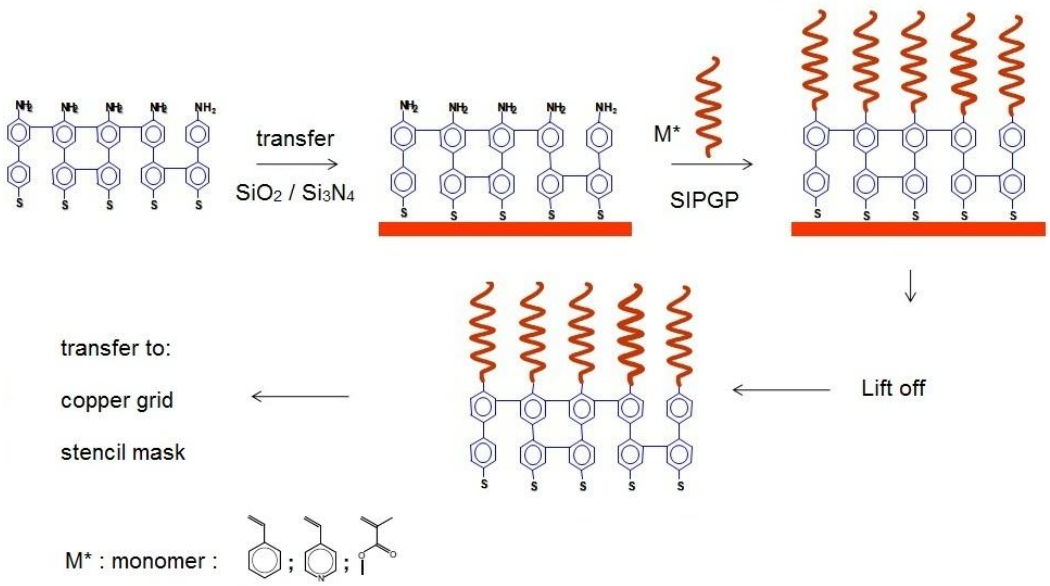

Figure 4.2. Schematic illustration of the SIPGP process on nanosheets and the transfer procedure for obtaining freestanding polymer carpets.

Freestanding nanosheets and carpets were fabricated by transfer from the substrates with silicon nitride (Si_3N_4) layers onto TEM Cu grids (400 mesh). For that purpose the polymer/SAM film was cleaved from the substrate by dissolving the silicon nitride layer in hydrofluoric acid (48%) as illustrated in figure 4.2.

4.2. Characterization Techniques

4.2.1. X-ray photoelectron spectroscopy

XPS characterization was always performed directly after deposition of the monolayer. The spectra were recorded with an Omicron Multiprobe spectrometer using monochromatic Al Ka radiation. The XP spectra were calibrated by setting the Au $4f_{7/2}$ signal to 84.0 eV. XP spectra were fitted by using symmetric voigt functions with shirley background correction.

4.2.2. Atomic Force Microscopy

Atomic force microscopy (AFM) scans were performed under ambient conditions by using a Nanoscope IIIa scanning probe microscope (Veeco Instr., Mannheim, Germany) using standard tips in tapping mode under ambient conditions. For the AFM measurements in liquids (water, ethanol) at room temperature, we used a

MFP-3D (Atomic Force, Mannheim, Germany) with a standard liquid cell. Scans were performed in tapping mode and with standard tips. The measurements of the Young's modulus of the nanosheets and polymer carpets were performed with a home-made setup described previously[8] on a NTEGRA atomic force microscope from NT-MDT (Eindhoven, The Netherlands).

4.2.3. Scanning electron Microscopy

The SEM measurements were acquired using a LEO 1530 scanning electron microscope. The electron beam energy was set at 3 keV, vacuum pressure ~5 x 10^{-6} mbar. The secondary electrons were detected with an in-lens-detector.

4.2.4. Contact Angle Measurement

The water contact angle measurements were performed by using a full automated Krüss DSA 10 Mk2 contact angle goniometer. The data were acquired with the aid of the Krüss Drop Shape Analysis v3 software package.

4.2.5. Infrared spectroscopy

For infrared spectroscopy we used a Bruker, IFS 55 with a liquid nitrogen cooled MCT-detector. Polarization filter Spectral resolution: 4 cm^{-1}. The infrared measurements of the polymer grafts were recorded using a diffusion reflectance Fourier transformed **(**DRIFT) setup from Spectra Tech. 550 scans were accumulated. Attenuated total reflection Fourier transformed infrared (ATR-FTIR) measurements were performed with a ZnSe crystal from Spectra Tech.

5. Results and discussion

5.1. Fully cross-linked chemically patterned monolayers

Nanoscale objects with chemically patterned surfaces are key elements in the development of novel functional devices. A promising fabrication strategy utilizes self-assembled monolayers (SAMs) of aromatic molecules[1-4] to coat the surface of an object with molecules carrying well defined functionalities. We have developed a method to fabricate mechanically stable self-assembled monolayers (SAMs), which we can further chemically functionalize.

5.1.1. Fabrication of FCCP SAMs

A general method for fabricating A FCCP SAMs is introduced. A FCCP monolayer can be fabricated by exchanging two different aromatic molecules. The method consists of: (i) patterning of the first type of aromatic molecules. A shadow mask is used by which cross-linked and non-cross-linked areas are generated, (ii) immersion of the patterned sample in a solution of a second aromatic compound. This results in an exchange between the first type of aromatic molecules on the

non-cross-linked region and the second one. (iii) irradiation of the exchanged sample results in a fully cross-linked monolayer.

In the beginning of our study for the fabrication of FCCP SAMs, a SAMs of BPT patterned has been used, where the non-cross-linked area was exchanged with NBPT molecules.

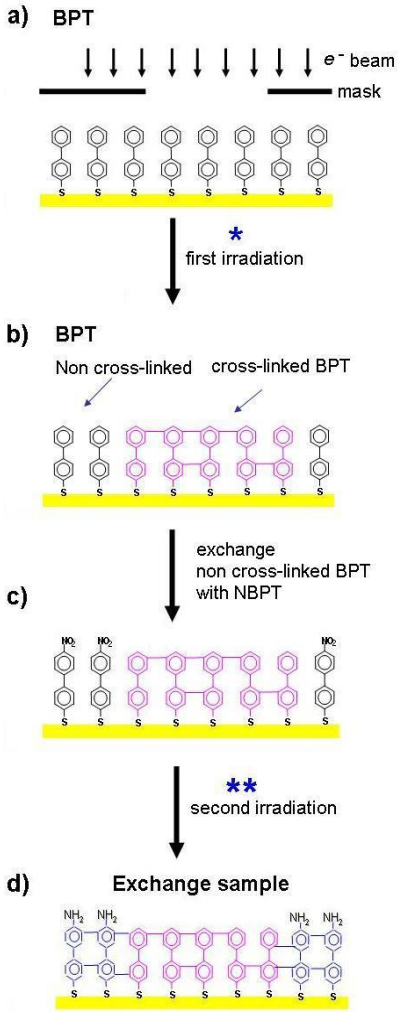

Figure 5.1 Schematic fabrication of an exchange sample. First, a BPT sample is patterned using a shadow mask with an irradiation dose of 20 mC/cm^2 (a-b). This generates cross-linked and non-cross-linked regions. Immersion of the patterned BPT sample in a NBPT solution leads to the exchange of non-cross-linked BPT with NBPT (c). Finally, irradiation of the entire surface with a dose of 40 mC/cm^2 leads to a fully cross-linked monolayer (d).

To confirm that an exchange had taken place, XPS was done. Figure 5.2 shows the XPS result of an exchange sample at room temperature (T_R). We have observed the exchange process after 24, 48 and 72 hours; the exchange takes place after 72 hours as the nitrogen peak and oxygen peak then become apparent.

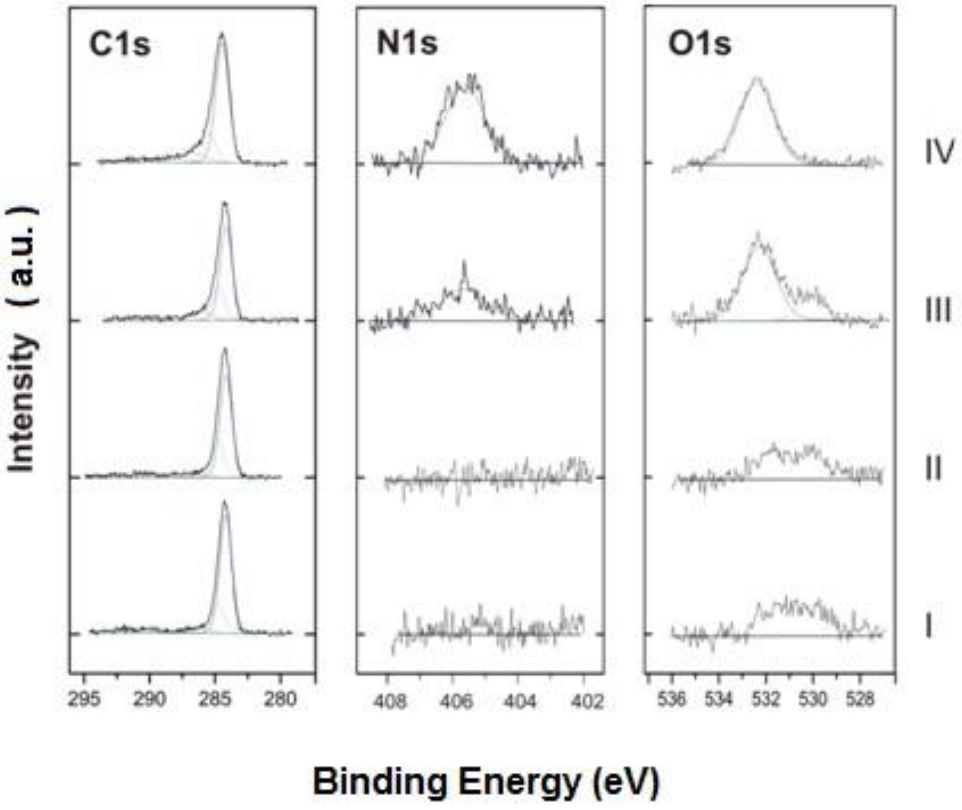

Figure 5.2 XPS spectra of an exchange sample at room temperature. (a) Carbon peak, (b) Nitrogen peak, (c) Oxygen peak. Curve I, II, III and IV immersion of BPT SAM after 0, 24, 72 h in a NBPT solution, and direct NBPT deposition for 72 h, respectively.

However, the nitrogen peak (III) shows that we do not have a perfect monolayer as the intensity of the nitro-peak is smaller than that of the exchange sample (III) compared to direct deposition NBPT SAMs (IV). The strategy to improve this result is to increase the temperature during the exchange process. It is well known

that an increased temperature during deposition of SAMs can speed up the adsorption process since the reaction rate is enhanced. For further investigation, we have performed the exchange process at the higher temperature of 55 ℃.

For our fabrication process two processes have been used, as shown schematically in fig. 5.3.

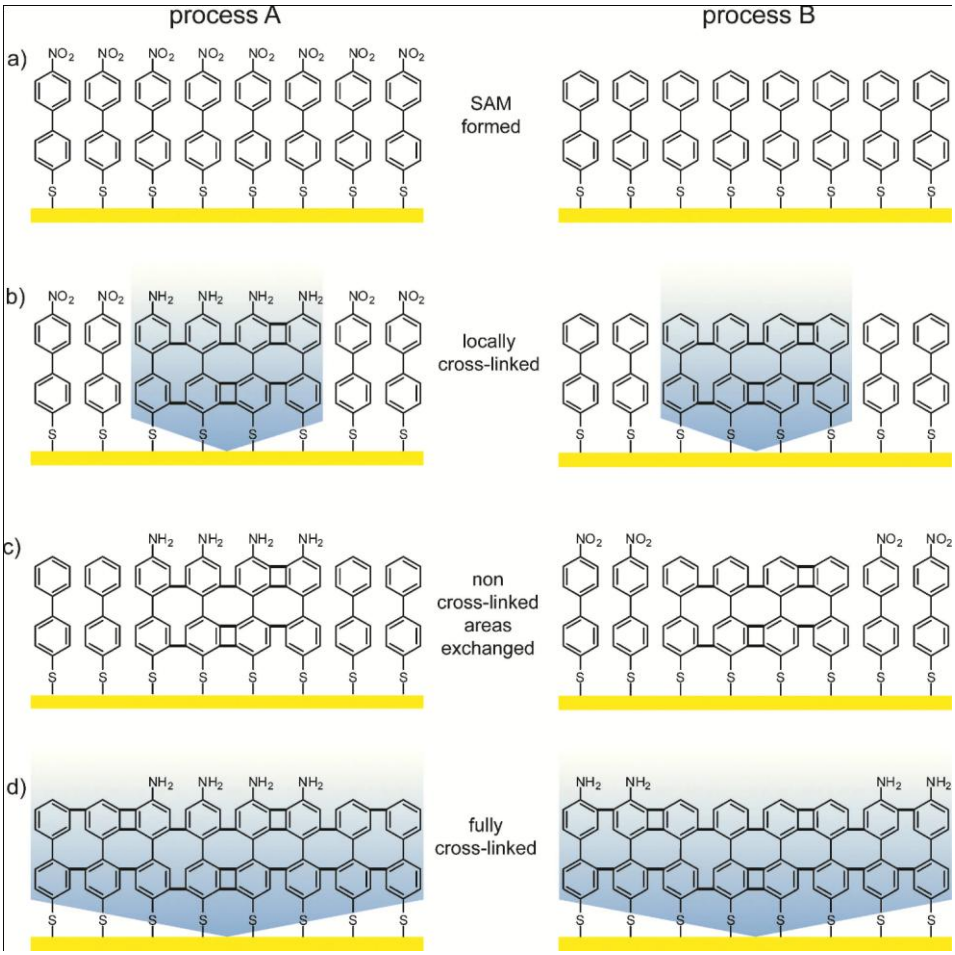

Figure 5.3 The fabrication of FCCP SAMs. (a) The process starts with deposition of NBPT SAMs on a gold surface for process A and BPT SAMs for B. (b) Local electron irradiation of SAMs is done, generating patterns between cross-linked and non-cross-linked regions, (c) In non-cross-linked regions of SAMs, thiols are exchanged with other biphenyl SAMs, (d) Final electron irradiation. This procedure results in a fully cross-linked monolayer.

In process A, a SAMs of NBPT is deposited on a gold surface. Next, the SAMS is irradiated with electrons whilst a carbon quantifoil mask is placed on the NBPT SAMs. This leads to intermolecular cross-linking and conversion of nitro functionalities to amino groups within the exposed area, generating patterns. During the immersion of patterned NBPT SAMs in a solution of BPT in DMF, the non-cross-linked NBPT molecules are exchanged by BPT molecules. A fully cross-linked SAMs is achieved by electron exposure of the entire surface. A positive pattern is defined, if the first electron irradiation patterns the chemically active amino groups and the second irradiation performs the cross-linking of surrounding areas. By a similar fabrication process, a negative patter can be generated, starting with BPT SAMs and exchanging non cross-linked BPT molecules with NBPT molecules after the first electron irradiation. A final electron irradiation of the entire surface results in cross-linking of NBPT SAMs, converted nitro to amino groups and linking the amino groups to a non-functionalized BPT area.

To check that both fabrication processes actually occur, the exchange and exposure processes have been monitored by XPS. In both processes, SAM-covered samples have been immersed in a 10mM solution of thiols in DMF at 55℃. Fig. 5.4a shows XP-spectra of the positive process A.

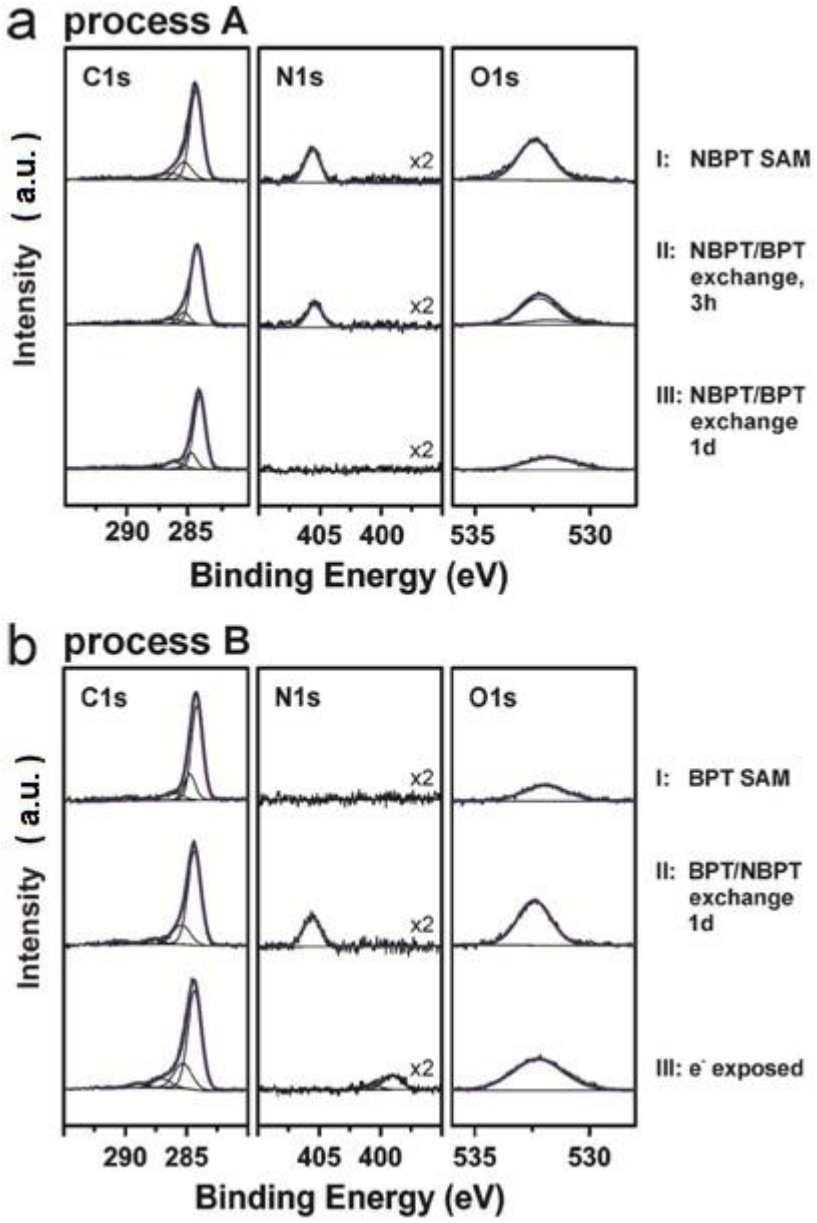

Figure 5.4 XPS monitoring of thiol exchange. (a) Process A: (I) SAM of NBPT obtained by self-assembly on a bare gold surface; (II) after 3 hours of immersion in a solution of BPT in DMF at 55℃, the monolayer still contains ~70% NBPT; (III) after one day of immersion, NBPT has completely been replaced by BPT. (b) Process B: (I) BPT monolayer obtained by self-assembly on a bare gold surface; (II) after one day of immersion in a solution of NBPT in DMF at 55℃, the BPT SAM is almost completely (~90%) replaced by NBPT; (III) electron irradiation converts the nitro into amino groups.

The top spectra (Fig 5.4 a, I) were obtained from an unexposed NBPT monolayer. The C1s signal consists of peaks at 284.3 eV (FWHM = 1.2 eV) and 285.3 eV (1.6 eV), and of two shake-up satellites at 286.4 eV and 290.5 eV (1.9 and 1.5 eV). The peak at 284.3 eV is assigned to the carbon atoms of the biphenyl except for the ones bound directly to sulfur and nitrogen, which are attributed to the peak at 285.3 eV. As in an earlier XPS study of NBPT[104], the N1s and O1s signals are found at 405.6 eV (1.5 eV) and 532.4 eV (1.9 eV), respectively. The XP-spectra of a NBPT SAM after 3 hours of immersion in a solution of BPT (II) reveal a noticeable drop of the intensity of the N1s and O1s peaks. However, they are still clearly detectable, which indicates that the NBPT was replaced only partially by BPT. To quantify the degree of exchange, we calculated the intensity ratio I (N1s)/ I (C1s) = I_{NC} of the nitrogen and carbon XP-signals. A well-ordered NBPT SAM has an $I_{NC} = 0.125 \pm 0.017$. After 3 hours of immersion in a solution of BPT this value dropped to $I_{NC} = 0.09$. Hence, we conclude that ~30% of the NBPT molecules were replaced with BPT. The bottom spectra in Fig. 5.4a (III) are obtained from a NBPT SAM after one day of immersion in a solution of BPT. Note that no nitrogen signal is detected, proving that all NBPT molecules were replaced by BPT. A low intensity O1s signal is found at 531.8 eV (2.5 eV). This is most likely due to adsorption of water onto the monolayer while washing the sample with DMF and ethanol and handling the sample in air. The Xp-spectrum is almost identical (C1s signals at 284.1 eV (1.1 eV) and 284.7 eV (1.1 eV), shake-up satellites at 286.1 eV (1.7 eV) and 289.8 eV (1.7 eV), O1s at 531.8 eV (2.5 eV)) to that of a BPT SAM (Fig. 5.4, top) prepared on a bare gold surface. This demonstrates the

practicability of molecular exchange of NBPT for BPT SAMs. The reverse process that exchanges BPT molecules for NBPT molecules was also investigated and monitored by XPS (Fig. 5.4b). The middle spectra in Fig. 5.4b originate from a BPT SAM after being immersed in a solution of NBPT for one day. The C1s, N1s and O1s intensities are similar to those of a NBPT SAM. From I_{NC} = 0.11 we conclude that ~90% of BPT molecules were replaced by NBPT. No exchange was detectable after 1 day, when working at room temperature instead of 55°C. To test whether a NBPT SAM, that is made by molecular exchange, has a similar sensitivity towards electron irradiation as a NBPT SAM, that is made by thiol adsorption on a bare gold surface, an exchange sample has been tested by electron exposure of 40 mC/cm^2. In the bottom spectra of Fig. 5.4b, the conversion of nitro to amino groups is visible by the disappearance of the nitro signal at 405.6 eV and the appearance of an amino signal at 399.0 eV with a shoulder at 400.4 eV. This clearly demonstrates that NBPT SAMs made by molecular exchange can be used for electron induced chemical lithography[92] in the same way as ''conventional'' NBPT SAMs are made by adsorption on a bare surface

To optimize the fabrication of biphenyl SAMs via molecular exchange, the kinetics of the exchange reaction was determined. Figure 5.5 shows the normalized XPS intensity ratios R_{NC} as a function of exchange time for process A and B. The nitrogen to carbon intensity ratios have been normalized with the value of a conventional NBPT SAM:

$$R_{NC} = I_{NC} \text{ (after exchange)} / I_{NC} \text{ (NBPT SAM)} \quad \text{(Eq. 5.1)}$$

The C and N intensity ratios can thus be regarded as a measure for the concentration of NBPT molecules in the monolayer. Both exchange processes can be fitted assuming Langmuir type kinetics. For process A, we fit the measured R_{NC} values to the equation:

$$R_{NC} = \exp(-k_m * t) \quad \text{(Eq. 5.2)}$$

where the exchange rate constant $k_m = (0.22 \pm 0.04)\ h^{-1}$ is obtained. For the reverse process B, we fit R_{NC} to the equation:

$$R_{NC} = 1 - \exp(-k_m t) \quad \text{(Eq. 5.3)}$$

For this process B, we obtain $k_m = (0.07 \pm 0.02)\ h^{-1}$, which is roughly three times lower than the k_m for process A.

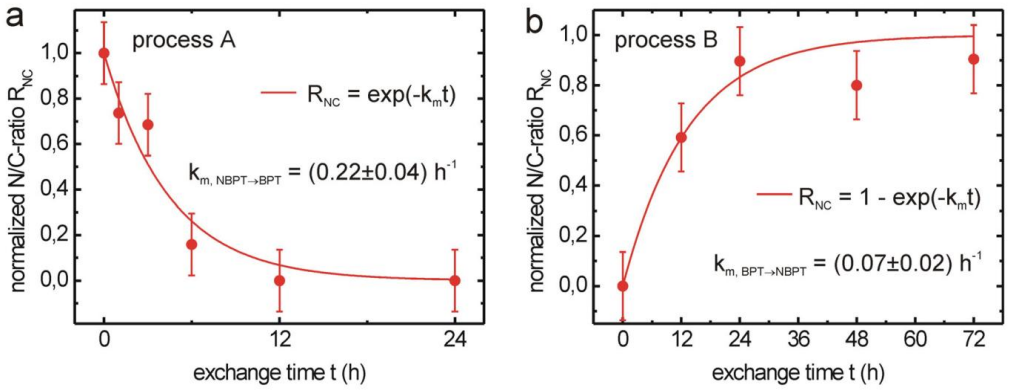

Figure 5.5 Kinetics of the exchange of NBPT for BPT (process A) and of BPT for NBPT (process B) in DMF at 55°C based on XPS data. The nitrogen/carbon-ratio R_{NC} denominates I_{NC} (after exchange) normalized to the value of I_{NC} for a NBPT SAM. Fitting the data with the equations for Langmuir kinetics yields a three-times-higher exchange rate constant k_m for process A in comparison to process B.

An AFM image (contact mode) of such a FCCP monolayer made by process A is shown in Fig. 5.6a.

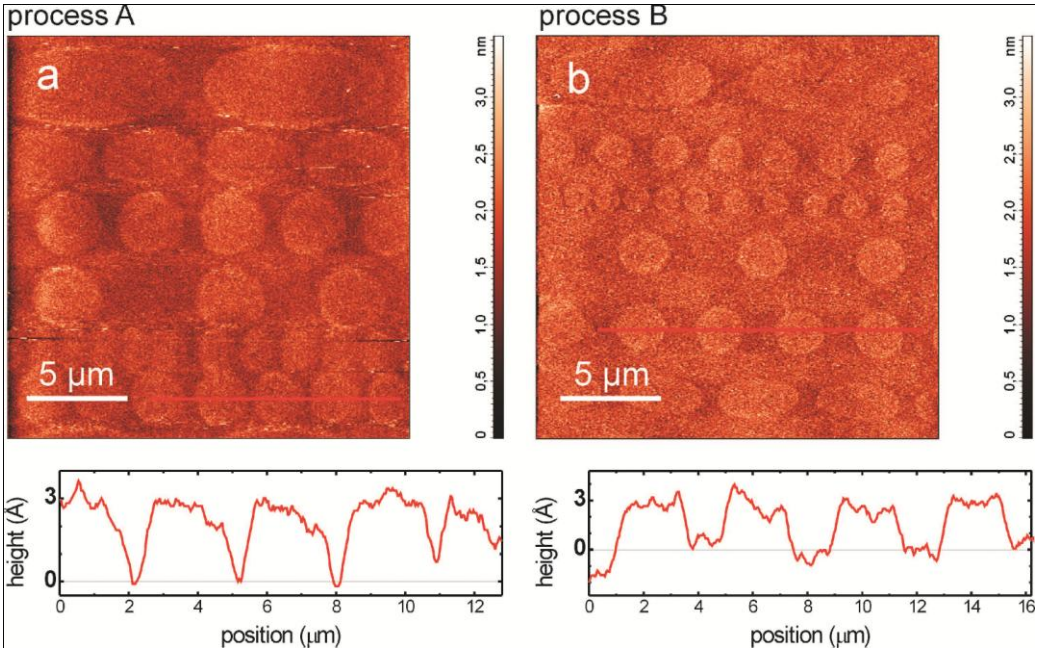

Figure 5.6 (a) AFM image (contact mode) showing the topography of a fully cross-linked, chemically patterned monolayer obtained through process A. The amino terminated areas (inside the circles) appear higher by ~ 3 Å in comparison to the BPT areas (outside the circles). (b) AFM topography of a fully cross-linked chemically patterned monolayer obtained by process B. For the next step, a surface functionality test on our FCCP monolayers has been performed.

The interior of the circles appears ~3 Å higher than the surface of the adjacent regions. This AFM contrast is assigned to differences in stiffness. It is known that cross-linked SAMs are stiffer than non-cross-linked ones.[94] As the regions within the circular openings were exposed to electrons twice, with a total dose of 60 mC/cm^2, they contain more cross-links and are therefore stiffer than the regions outside the circles that only had a single exposure of 40 mC/cm^2. This interpreta-

tion of the AFM contrast is supported by Fig. 5.6b which shows the topographical AFM image of a FCCP monolayer with a negative chemical pattern that has been fabricated using to process B. Here the cross-linked non-functionalized regions are inside, whereas the amino terminated regions are outside of the circles. Nevertheless the AFM image shows the same topography, i.e. the interior of the circles appear ~3Å higher than the regions outside. Hence, the AFM contrast reflects the difference in the electron irradiation dose.

5.1.2. Functionalization of FCCP SAMs

Functionalization of our FCCP samples, both positive and negative patterns is performed. We treated our FCCP layers with pentanoic acid chloride in the presence of ethyldiisopropylamine in 1,2-dichloroethane solvent. The process results in amide formation at the amino terminated ends. The corresponding AFM images in fig. 5.7 show a height increase of the amino terminated regions, as expected. This demonstrates that both types of FCCP monolayers can be functionalized. After functionalization, in a positive pattern (Fig. 5.7a), we observed a difference in thickness between the amino terminated and non-functionalized region of around 10 Å. The same result is found for a negative pattern (fig. 5.7b). This confirms the suggestion that the AFM height profile of FCCP monolayers before functionalization with acid chloride is mainly due to differences in mechanical

stiffness. The AFM images in fig. 5.7 clearly show that the functionalization of both types of FCCP monolayers can be performed.

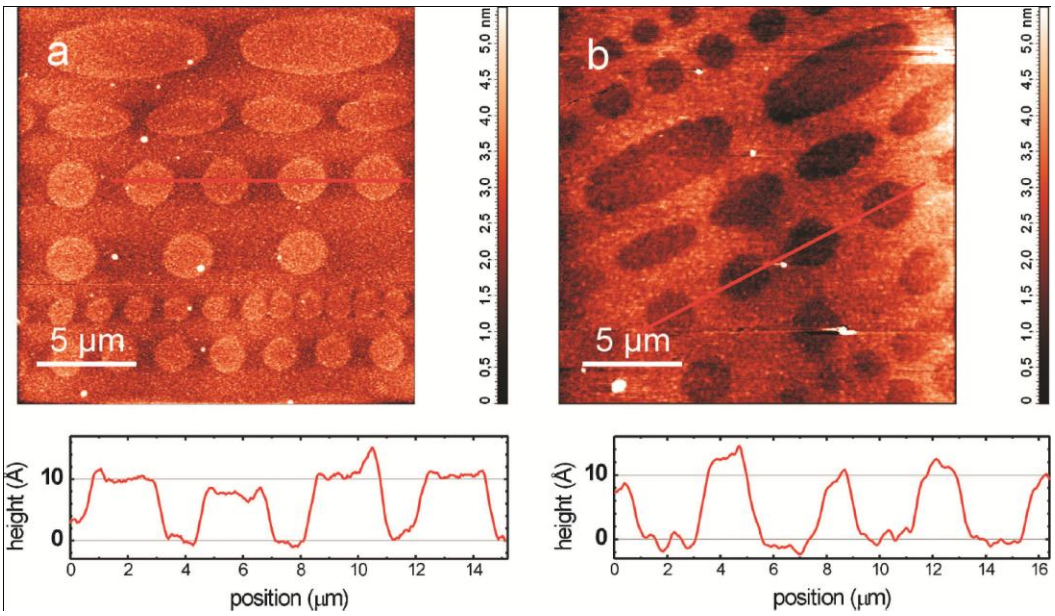

Figure 5.7 AFM images (contact mode) showing the topography of a fully cross-linked and chemically patterned monolayer after treatment with pentanoic acid chloride in the presence of ethyldiisopropylamine. (a) Process A furnishes SAMs with the amino terminated areas inside the circles. (b) Process B resulted in SAMs with the amino terminated areas outside of the circles.

5.1.3. FCCP nanosheet

The mechanical stability of the fully cross-linked, chemically patterned monolayer was demonstrated by transferring it to another substrate. This technique was recently introduced for the preparation of cross-linked freestanding SAMs as sample support for transmission electron microscopy.[101] By dissolution of the gold sub-

strate, the bonds between the cross-linked monolayer and the substrate were cleaved and the monolayer was detached, resulting in a nanosheet. The nanosheet can be transferred to a silicon dioxide substrate or TEM grid for making it freestanding. For our purpose, we transferred the detached monolayer on a silicon dioxide surface. This allowed the inspection of the monolayer by optical microscopy. [105] As shown in figure 5.8b a pattern is hardly recognizable, but it shows that a homogeneous monolayer over an area of several millimeters was transferred.

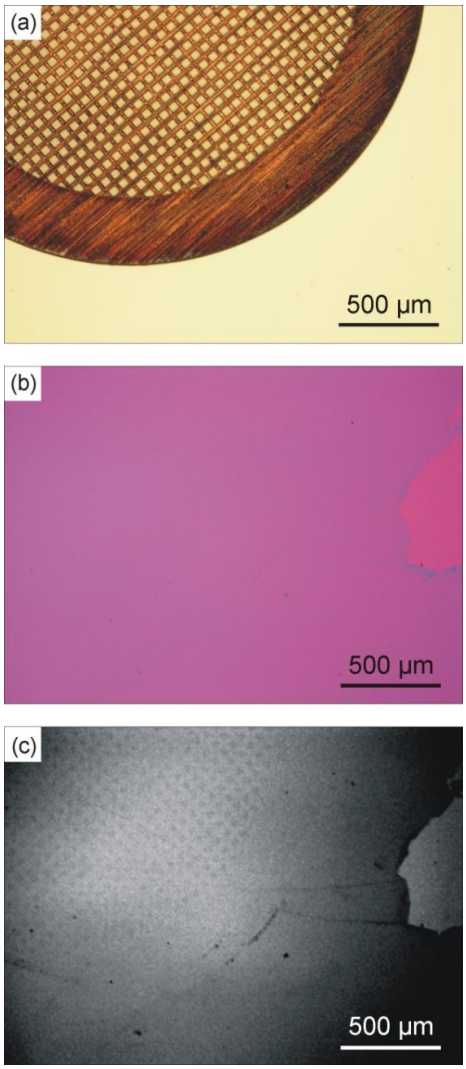

Figure 5.8. Optical microscopy images: (a) Stencil mask used for imposing a pattern into BPT monolayer. This copper grid is coated by a 20 nm thin carbon foil with micron-sized elliptic and circular openings. (b) A fully cross-linked, chemically patterned monolayer after transfer onto a silicon dioxide surface. The monolayer covers almost the complete millimeter-sized field of view except for a small region on the right side. (c) The pattern within the monolayer becomes visible after a contrast enhancement. The BPT areas (circles and ellipses) have a slightly higher contrast, which indicates an increased refractive index or a higher thickness. This is consistent with the AFM images.

The same image is shown in figure 5.8c after a substantial enhancement of the contrast. Here, the chemically patterned part of monolayer generated by the stencil mask is visible. The weak contrast in figure 5.8b might originate from the difference in the electron dose which may have led to a slight difference in the refractive index. This is consistent with the AFM topography image which indicated small differences in the stiffness of areas of cross-linked BPT and amino-BPT due to the difference of the electron dose. Important to note is the absence of any rupture in the monolayer. The crosslinking must have worked well even at the border between the already cross-linked BPT and the freshly assembled NBPT areas, so that the whole monolayer is sufficiently stable to withstand the transfer process.

Functionalization of our FCCP nanosheet is also performed with a positive pattern nanosheet. The nanosheet was treated with pentanoic acid chloride in the presence of ethyldiisopropylamine in 1,2-dichloroethane solvent, exactly the same treatment as our FCCP monolayer on gold substrate. Fig. 5.9a shows an AFM image of the positive pattern nanosheet before functionalization. A height difference of 3.2 Å between the amino terminated areas (inside the circles) and the cross-linked BPT areas (outside the circles) was observed. This result is in a good agreement with the value obtained for the FCCP monolayer on gold substrate. After functionalization, the height of amino terminated areas increased. We observed a difference in thickness between the amino terminated and the non-functionalized region of around 10 Å. This result is again in a good agreement with the value obtained for the FCCP monolayer on a gold substrate. This demonstrates that FCCP nanosheets can be functionalized.

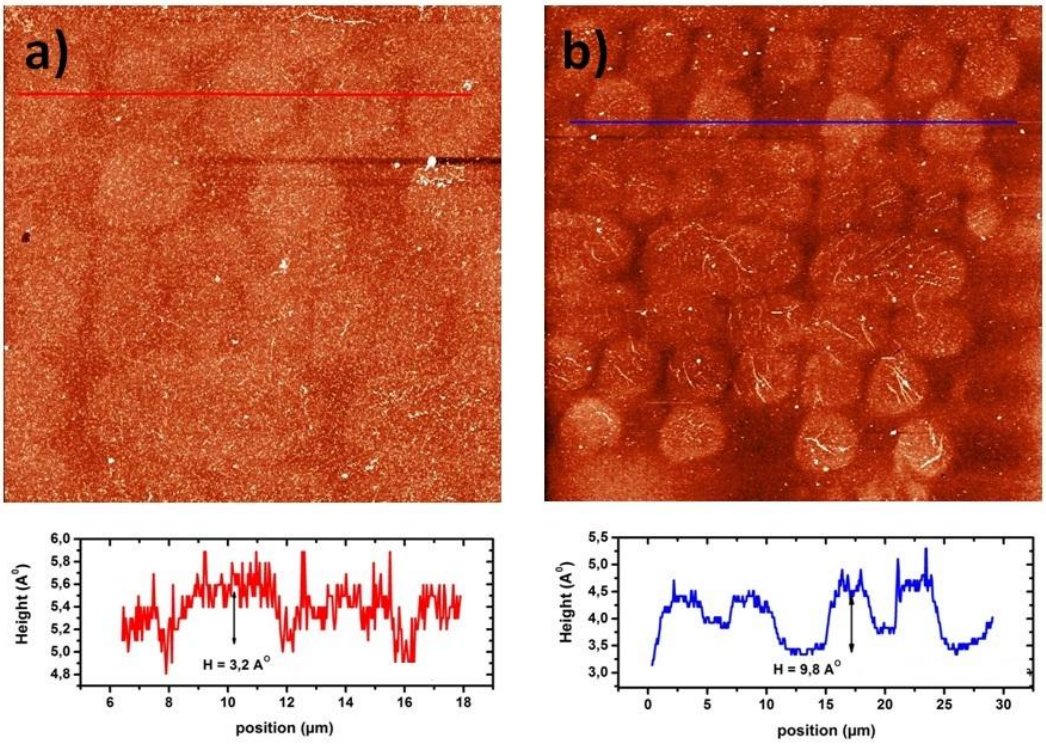

Figure 5.9 AFM images of positive pattern FCCP nanosheet: a) before b) after functionalization with pentanoic acid chloride in the presence of ethyldiisopropylamine in 1,2-dichloroethane solvent.

To our best knowledge, this is the first report on the fabrication and functionalization of two-dimensional patterned nanosheets.

5.1.3 Summary

This fabrication process has clearly shown that a chemically and mechanically stable 2 dimensional patterned nanosheet can be achieved. Further functionalization of the fully cross-linked monolayer is possible. The mechanical stability of

the fully cross-linked chemically patterned monolayer was demonstrated by transferring it to another substrate. These layers may find a variety of technical applications as mechanically stable chemically functional surfaces.

5.2 Freestanding polymer nanosheets

Freely suspended thin and flexible polymeric membranes, with molecular scale thicknesses combined with macroscopic lateral size, are continuously gaining significant scientific and industrial interest due to their enormous potential applications to create a variety of smart, switchable and multifunctional surfaces with extraordinary sensitivity and dynamic range; microsensors, actuators or separation membranes.[106-108] Many strategies have been developed to fabricate defect-free and mechanical robust freely suspended ultrathin polymeric membranes. Layer-by-layer (LbL) assembly of polyelectrolyte multilayers[109, 110], crosslinking of Langmuir-Blodgett[111] and self-assembled monolayers (SAMs)[96, 102], self-assembly of ABA triblock copolymers[112] and cast films[113]. More recently, efforts have concentrated on enhancing the mechanical stability and elasticity of these polymeric nanomembranes. Tsukruk et al.[114, 115] showed that very robust 25-70 nm thick membranes were accessible by embedding rigid nanoparticles within polymeric nanomembranes prepared by LbL assembly. Kunitake et al.[116, 117] developed different approaches for the preparation of 20-40 nm thick, mechanical stable nanomembranes by “high-density crosslinking” of a spin-coated precursor solution. Due to their extraordinary sensitivity and dynamic range, these highly cross-linked nanomembranes are very promising candidates for the next-generation of membrane-based pressure, thermal, tactile and acoustic sensors[118, 119], and in biomedical field as artificial nacre[120] and as novel material used in surgery[121]. However, for the fabrication of chemical- or bioresponsive polymeric

nanomembranes, “high-density crosslinking” is one major inconvenience since this drastically reduces the interaction between the polymer chains and the adjacent liquid or gas phase. More flexible polymer chains would allow the penetration of the mobile phase into the polymer layer and enable interaction of (bio)-molecules with binding sites within the layer. In the past decade, such soft and stimuli responsive polymer layers have been prepared widely on solids via polymer brushes. Soft and stimuli responsive polymer brushes have been the system of choice for the development of adaptive layers as actuators and sensors.[8,122-125]

Here, we report on the preparation of the first freestanding polymer brush by grafting polymers on a cross-linked nanosheet. A nanosheet that provides the mechanical stability and structural integrity was used as a 2D template to grow a polymer brush by surface-initiated photografting photopolymerization (SIPGP), forming the a so-called polymer carpet. Freestanding polymer carpets are obtained by dissolving the underlying solid substrate.

5.2.1. Grafting polymer brushes on homogenous nanosheet

Recently, Steenackers et al. reported that a specific surface-bound initiator is not needed and polymer brushes of equal quality can be prepared by the self-initiated surface photopolymerization and photografting (SIPGP) of vinyl monomers. [100,126, 127] This straightforward and easy approach has been applied for the preparation of polymer brushes on crosslinked biphenyl nanomembranes (Fig. 5.10a).

First, a ~1 nm thin nanosheet is prepared by electron beam induced crosslinking of a biphenyl SAM. It was shown recently that these macroscopic large and ultra-thin nanomembranes are extremely stable, mechanically and thermally.[102] In a second step, polymer brushes are grafted on the cross-linked biphenyl nanomembrane by SIP, forming a so-called polymer carpet.

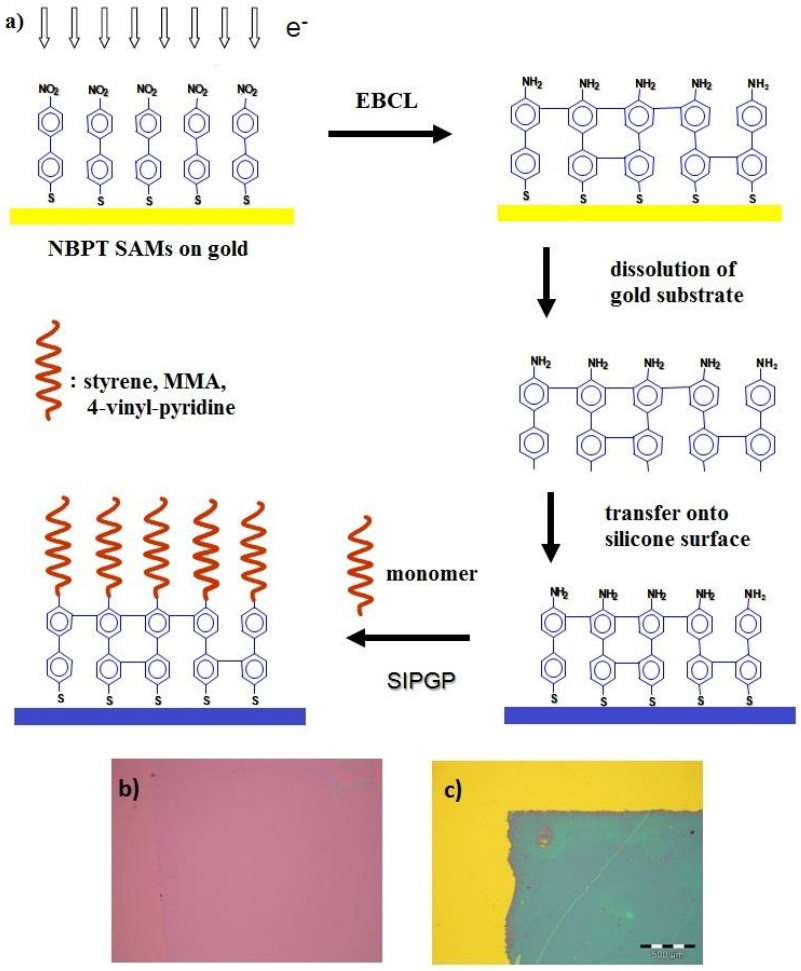

Figure 5.10 a) Schematic illustration of the preparation of polymer carpets. The electron irradiation of the 4'-nitro-1-1'-biphenyl-4-thiol (NBPT) SAM on gold results in a cross-linked 4'-amino-1,1'-biphenyl-4-thiol (cABPT) SAM. After dissolution of the gold substrate and deposition onto a silicon wafer, a cABPT nanosheet is obtained. Polymer carpets are obtained by SIPGP of a vinyl monomer on the cABPT nanosheet. Optical image of nanosheet (b) before c) after 4hr polymerization of styrene. Both are at the same scale.

The preparation of polymer brushes by SIP has been widely used during the past decade and various strategies have been developed for the immobilization of surface-bonded initiators on substrates.[8, 123]

In a first set of experiments, polystyrene (PS) carpets were prepared by the SIPGP of styrene on approximately 5x5 mm^2 cross-linked 4'-amino-1,1'-biphenyl-4-thiol (cABPT) nanosheets deposited on 9x9 mm^2 silicon wafers. The cABPT/silicon substrates were submerged in styrene and irradiated with UV light for different times (0.5-16 h). The substrates were then intensively rinsed with solvents of different polarities, dried in a jet of nitrogen, and investigated by AFM under ambient conditions. PS was selectively grafted on the cABPT nanosheets and no polymer was observed on the bare silicon wafer. The difference in reactivity between the native silicon substrate and the cABPT nanosheet is in agreement with previous reports.[100, 126, 127]

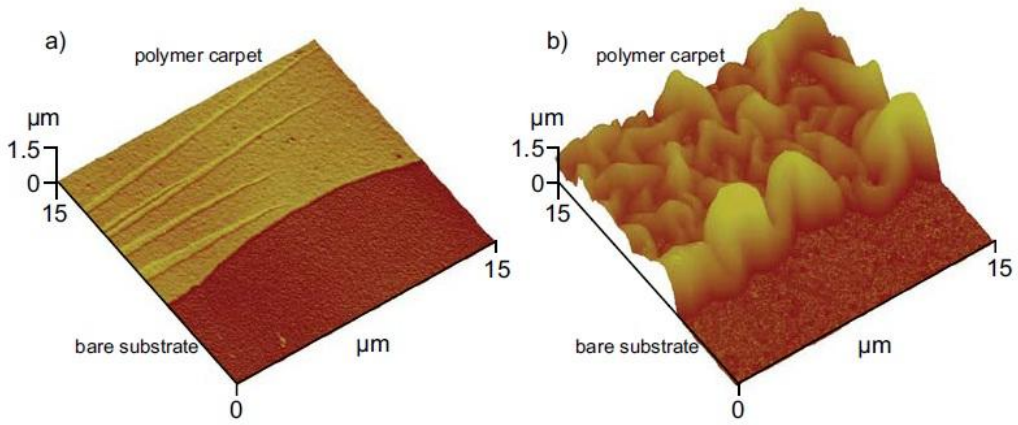

Figure 5.11 True to scale 3D representations of AFM measurements of PS carpet edges on silicon. a) UV irradiation time: 0.5 h; PS nanocarpet thickness: 19 ± 7 nm. b) UV irradiation time: 16 h. Here, the PS nanocarpet thickness could not be determined accurately by AFM due to the high buckling amplitude (approximately 1.5 µm rms).

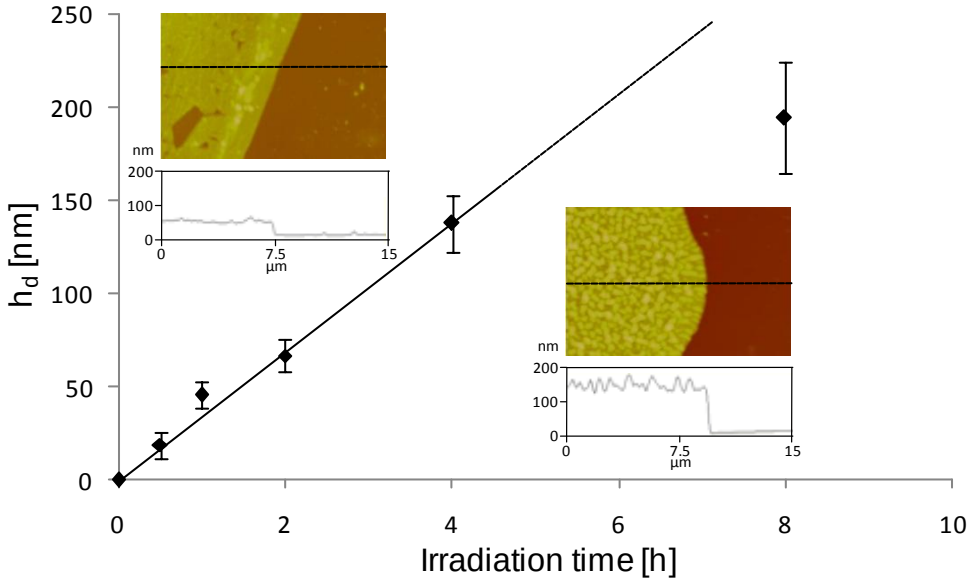

Figure 5.12 Thickness of the dry PS carpets (h_d) as a function of the UV irradiation time. (λ_{max} = 350 nm) on cABT nanosheets on silicon as measured by AFM. The insets show AFM height images and section analysis of PS carpet edges after a polymerization time of 1 h (left) and 4 h (right).

Ex situ kinetic studies of the SIPGP of styrene were performed on individual cABPT/silicon samples after different UV irradiation times (0.5-16 h). In Figure 5.12, the dry PS carpet thickness (h_d) is plotted as a function of the UV irradiation time. The thickness of the PS carpets was determined by AFM measurements on the carpet edges.

For polymerization times below 4 h, an almost constant growth rate of 35 $nm.h^{-1}$ is observed. However, the growth rate of the carpet thickness decreases at longer polymerization times. This behavior is in agreement with previous reports on SIPGP.[128] These kinetic investigations show that the polymer membrane thick-

ness can be very precisely controlled over a wide range, by varying the polymerization time.

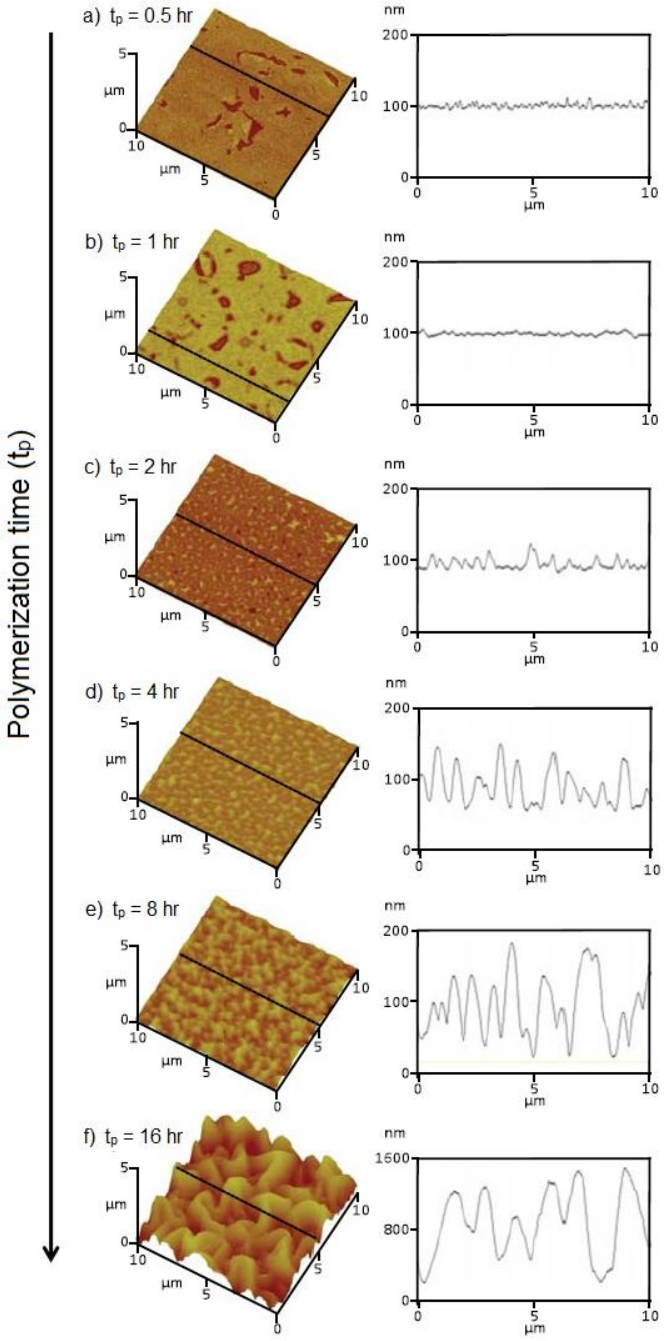

Figure 5.13 True to scale 3D representations and section analysis of AFM measurements of PS carpet prepared by the SIPGP of styrene on cABT nanosheets on silicon for (a) 0.5 h, (b) 1 h, (c) 2 h, (d) 4 h, (e) 8 h and (f) 16 h.

Investigations by AFM of the PS carpets' morphology revealed that at polymerization times below 1 h, homogeneous and very flat films were formed with a roughness of less than 2.5 nm rms (Figure 5.13a-b). However, at longer polymerization times, a significant increase in roughness of the PS carpet was observed. Figure 5.13 shows the formation of a wavy film structure with increasing buckling amplitude after longer polymerization times. This indicates that the film roughness is not due to e.g. inhomogeneous reaction conditions or contamination, but to buckling of the PS carpets. After a polymerization time of 16 h, the polymer carpet thickness could not be determined accurately by AFM measurements due to the high buckling amplitude (the surface roughness reached 575 nm rms). Figure 5.13 shows three-dimensional true to scale representations of the PS carpets after different polymerization times.

The PS carpets were further investigated by establishing the static and dynamic water contact angle. Table 5.1 shows that the static water contact angle (θ_s) and difference between the water advancing and receding contact angles (contact angle hysteresis: $\Delta\theta = \theta_a - \theta_r$) increases with the surface roughness. The advancing water contact angle is approximately 95° for a flat PS carpet. However, the PS carpet prepared by the SIPGP of styrene for 16 h is highly hydrophobic and has an advancing water contact angle of 146°. The results of contact angle measurement for all polymer carpets of different deposition time are shown in table 5.1.

Table 5.1.Contact angle measurement for all polymer carpets of different deposition time.

	polymerization time (h)	layer thickness (nm)	roughness rms (nm)	θ_s (deg)	θ_a (deg)	θ_r (deg)	$\Delta\theta$ (deg)
a)	0,5	19 ± 7	1,6	95	95	82	13
b)	1	46 ± 7	2,5	90	99	80	19
c)	2	67 ± 9	11	95	95	75	20
d)	4	138 ± 15	39	95	95	76	19
e)	8	195 ± 30	62	100	105	0	105
f)	16	-	575	135	146	0	146

Besides styrene, a broad variety of vinyl monomers can be grafted by the SIPGP process.[126, 135, 136] This allows for the preparation of polymer carpets with different properties and functionalities. Up to now, we have successfully tested methyl methacrylate (MMA) and 4-vinyl pyridine (4VP) on cABPT nanosheets. The growth rate of polymer carpet thickness was specific for each monomer and correlates roughly with the rate of polymerization of the monomer in solution. For example, after 3 h of irradiation, MMA gave a 485 ± 18 nm thick PMMA carpets and 4VP gave a P4VP carpet thickness of 150 ± 11 nm after 19 h of irradiation. The successful conversion of the cABPT nanosheets into PS, PMMA and P4VP was further confirmed by Fourier transform infrared (FTIR) spectroscopy (Fig. 5.14).

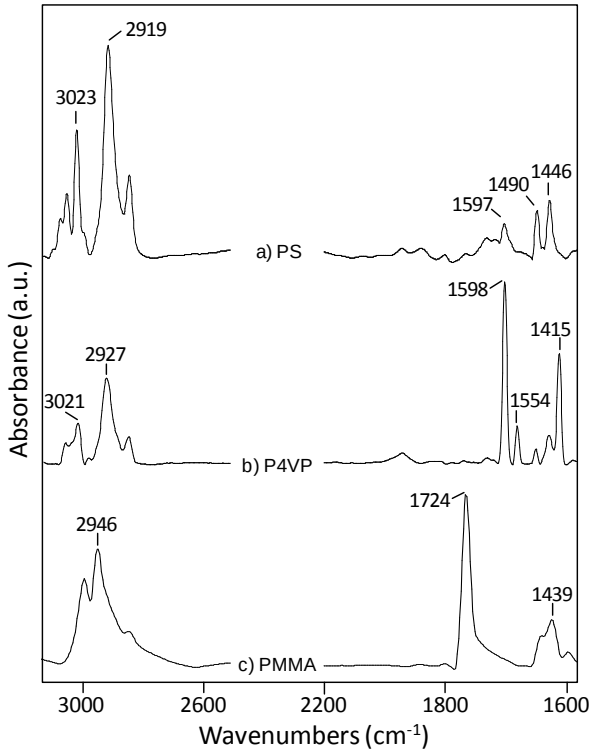

Figure 5.14 FTIR spectra of a) polystyrene, b) poly(4-vinyl pyridine) and c) poly(methyl methacrylate) nanocarpets prepared by the SIPGP of respectively styrene (irradiation time = 8 h), 4-vinyl pyridine (irradiation time = 19.5 h) and methyl methacrylate (irradiation time = 3 h) on cABT nanosheets deposited on a silicon wafer. The absorption bands are in agreement with the characteristic FTIR spectra for these polymers.

Buckling of thin supported films is well-known.[129] Especially strain induced buckling has been the subject of many studies.[130-132] In general, a thin film is adhered to a soft elastic substrate. Lateral compression of the substrate results in buckling of the film. Compressive stresses can be caused mechanically as well as thermally. The polymer carpets prepared by the SIPGP of vinyl monomers on cABPT nanosheets are comparable to these well studied systems. Polymer carpets are composed of a thin fully cross-linked and stiff biphenyl nanosheet on which

more flexible polymer brushes are grafted. The collapse of the polymer brush due to the changes in the environment (from bulk monomer and good solvents used for carpet cleaning to air) results in significant stress within the film. Such stress can occur due to the confinement effects in poor solvent conditions if the layer thickness is below the free extension of the chains.[133,134] In such a case the brush tends to develop instabilities which can at least partially be compensated by crumpling of a flexible substrate. Since the flexible polymer brush is linked to a cross-linked nanosheet that cannot compensate for the lateral stress, the entire carpet locally detaches from the rigid support and buckles. In other words, the buckling of these polymer carpets is caused by the lateral stress within this asymmetric layer due to swelling/collapsing of the polymer brush layer in good/poor solvents or in the dry state.

To verify this hypothesis, we investigated a P4VP carpet by AFM in 'good' and 'bad' solvents. P4VP carpets were prepared by the SIPGP of 4VP for 19 h on a cABPT nanosheet deposited on a native silicon wafer. After the polymerization, the substrate was thoroughly rinsed with ethanol and directly placed in an AFM liquid cell. The P4VP carpet was first measured in ethanol, which is a good solvent for P4VP (Fig. 5.15a). No buckling was observed here and a surface roughness of 5.1 nm rms was measured. However, when ethanol was replaced by water, clear buckling of the P4VP carpets could be observed and the surface roughness increased up to 273 nm rms (Fig. 5.15b). Water at neutral pH is a poor solvent for P4VP and causes the collapse of the polymer brushes. When placed in ethanol again, the P4VP unbuckled and a surface roughness of 5.0 nm rms was measured.

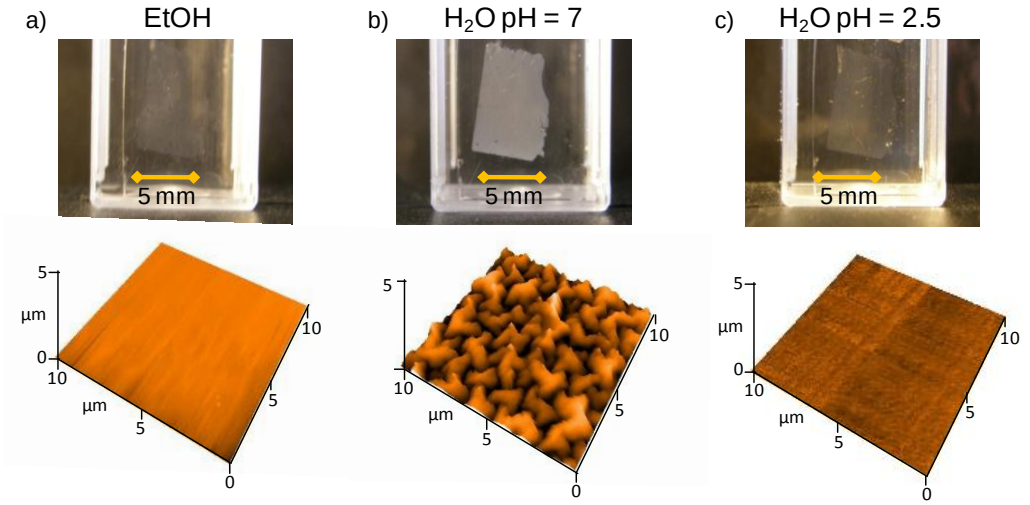

Figure 5.15 Photographs (above) and AFM measurements (below) of P4VP carpets in a) ethanol, b) water at pH 7 and c) water at pH 2.5.

Buckling and unbuckling the P4VP carpet by exchanging good and bad solvents was performed 3 times without any noticeable damage of the polymer layer, indicating a reversible transition. Apparently, the polymer carpets only buckle when the polymer brushes are in the collapsed state (in a poor solvent or in the dry state).

To investigate if this buckling/unbuckling transition is visible with the naked eye, we prepared -under identical reaction conditions- a P4VP carpet on a glass substrate. The optical photograph in Fig. 5.15a shows that P4VP carpet is almost invisible when placed in ethanol. However, the entire polymer carpet becomes clearly visible when placed in water due to the diffraction of light on the very rough polymer carpet surface. The same transition from invisible to visible was observed for PS carpets when placed in good or poor solvents. Furthermore, we observed in all experiments that the transition from a visibly buckled polymer

carpet to an invisible unbuckled carpet was instantaneous, indicating a very fast (sub-second) cooperative response of the entire membrane. In order to demonstrate the potential application of polymer carpet based sensors, we studied the effect of pH on a P4VP carpet. Fig. 5.15c shows that at a pH below the pK_a of P4VP, the polymer carpet unbuckles and becomes almost invisible. This is because below a pH of 5.5, the pyridine group is protonated and P4VP becomes soluble in water. However, when the pH increases above 5.5, the carpet buckles and becomes clearly visible again. This unexpected, fast, visible and reversible transition of polymer carpets toward a (chemical) stimulus could be applied in the development of new types of sensors or displays.

5.2.2. Freestanding homogenous polymer sheets

Freestanding polymer carpets with macroscopic lateral dimensions and thicknesses between 10 and 200 nm were prepared by a sacrificial layer approach as shown schematically in figure 5.16: First, the SIPGP of styrene was performed on 5x5 mm^2 cross-linked ABPT nanosheets absorbed on silicon wafers coated with a 100 nm thick sacrificial silicon nitride layer. The samples were successively immersed in an aqueous hydrofluoric acid (HF) solution to dissolve the sacrificial underlayer and release the polymer carpets. The entire 5x5 mm^2 self-supporting PS carpets floated in the aqueous solution and were easily transferable onto a copper trans mission electron microscopy (TEM) grid with hexagonal holes with a

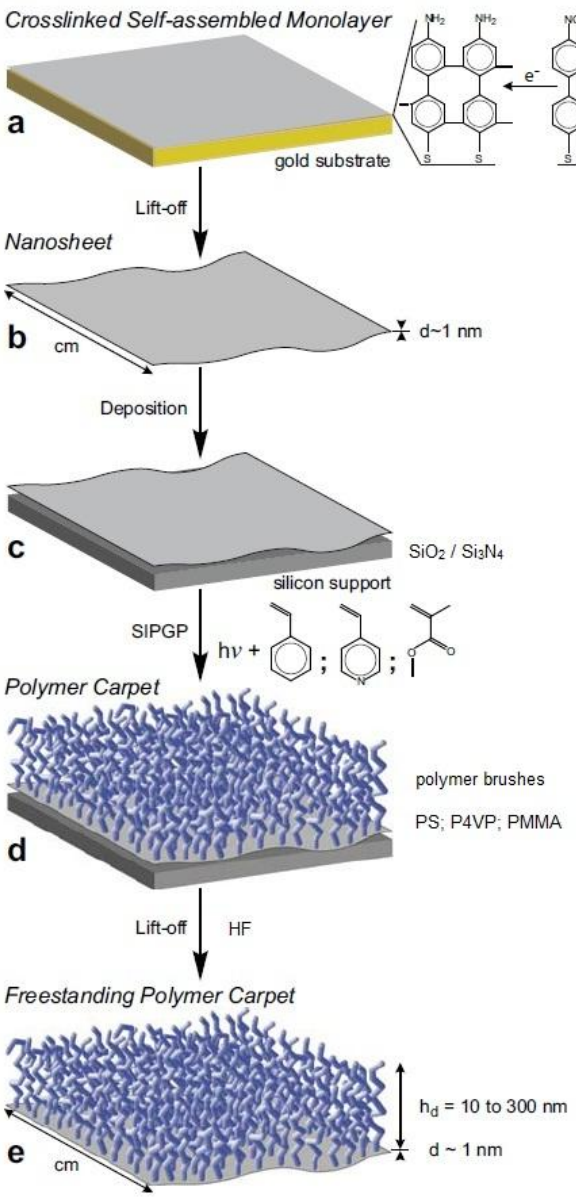

Figure 5.16 Scheme of the preparation of polymer carpets. a) A cross-linked 4'-amino-1,1'-biphenyl-4-thiol (cABPT) SAM is prepared by electron irradiation of 4'-nitro-1,1'-biphenyl-4-thiol (NBPT) and b) detached by dissolving the gold substrate with a KI/I_2 solution. c) The nanosheet is deposited on a silicon substrate with thin silicon oxide or silicon nitride layer. d) Supported polymer carpets are obtained by SIPGP of a vinyl monomer (styrene, 4-vinylpyridine or methyl methacrylate). e) Freestanding polymer carpets are obtained by dissolving the underlying layer (Si_3N_4) with HF.

diameter of 50 μm (Fig. 5.17) or onto a silicon substrate having a central micron-sized rectangular hole used for bulge tests (Fig. 5.18). It is noteworthy that these ultrathin free-standing membranes were robust enough to sustain solution treatment during transfer (aqueous HF, water and ethanol), high vacuum during TEM measurements, mechanical stresses during the mechanical tests and long storage (several months). Both optical and mechanical characterization of freestanding polymer sheets has been performed.

5.2.2.1 Optical characterization

The optical properties of freestanding polymer sheets are measured by determining the transmittance of polymer sheets with scanning transmission electron microscopy (STEM). Fig. 5.17 shows a photograph, optical micrograph as well as a scanning transmission electron microscopy (STEM) image of a PS carpet transferred onto a TEM grid. The optical micrograph (Fig. 5.17a) shows that the TEM grid holes are fully covered with the PS carpet without any defects or cracks. Fig. 5.17b shows the STEM image of a partially covered TEM grid opening at the carpet edge. Quantification of the electron intensities in Fig. 5.17c allows the calculation of the electron transmittance (T) through the PS carpet:

$$T = (I-I_B)/(I_0-I_B) \quad \text{.....(Eq. 5.1),}$$

where I, I_0 and I_B the electron intensities of the carpet, the uncovered opening and the copper bar shadow respectively. If the membrane thickness is known, the electron attenuation length, Λ, (which is inversely proportional to the mass density), can directly be derived from transmittance (T).

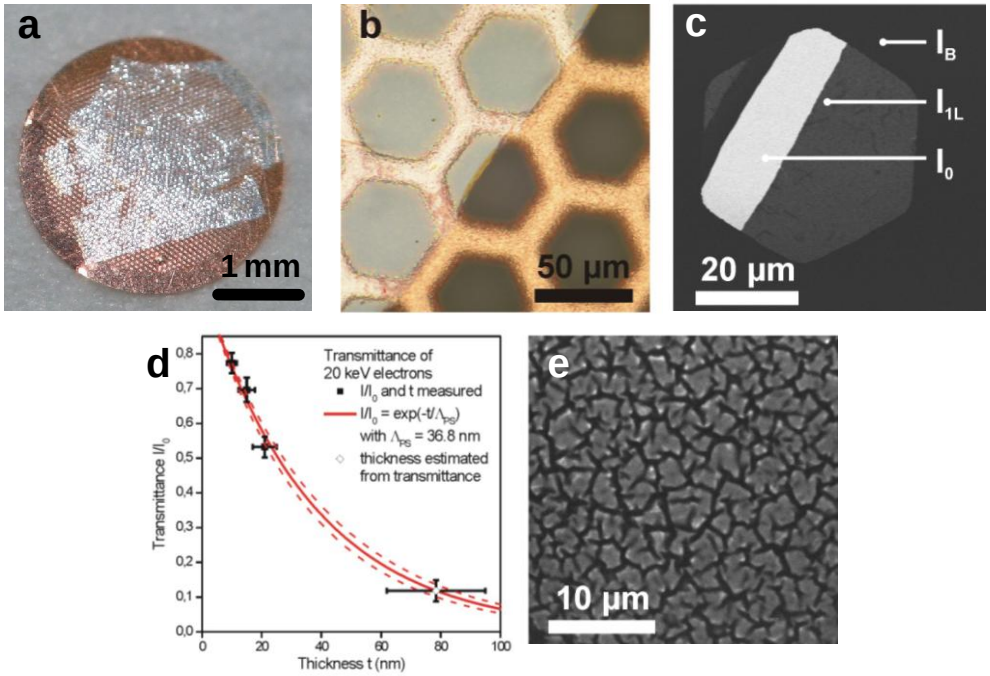

Figure 5.17 (a) Photograph, (b) optical micrograph and (c) STEM image of freestanding PS carpets. (d) The transmittance of 20 keV electrons was determined from STEM images of PS carpet edges such as in (c). An attenuation length (Λ_{PS}) of 36.8 nm (red solid line) ± 2.6 nm (dashed lines) was calculated. (e) STEM image of a freestanding PS carpet at higher magnification.

In Fig. 5.17d, T values are plotted as a function of the PS carpet thickness, which was previously measured by AFM. The electron attenuation length (at 20 kV) of PS carpets was found to be about 37 nm and independent of layer thickness. This is in agreement with the attenuation length of 20 kV electrons in bulk polystyrene

(40 nm)[137] and it can thus be concluded that the mass density of the PS carpets is almost identical to that of in bulk PS. It is noteworthy that also here, thicker polymer carpets could not be measured accurately by AFM due to the high buckling amplitude. However, assuming a constant attenuation length, electron transmittance measurements allows one to determine the layer thickness of thicker polymer carpets directly (Fig. 5.17d).

The STEM micrographs of thick freestanding PS carpets (>100 nm) in Fig. 5.17e show buckling of the layer. It is worth noting that for identical PS carpets, stronger buckling was observed for freestanding polymer carpets than for absorbed carpets. This indicates that Van der Waals interaction between the polymer carpet and the substrate probably partially inhibits the film from buckling.

5.2.2.2. Mechanical Behaviour

The micromechanical behaviour of polymer carpets was investigated using a bulge test setup. PS carpets of different thickness were transferred onto a silicon substrate with a central rectangular window of 30x40 μm^2. The samples were successively airtight mounted onto a home-build pressure cell[102] as shown schematically in Fig. 5.18a. A differential pressure between the two sides of the polymer carpet was applied and the resulting deflection was measured with AFM. Fig. 5.18a shows the resulting pressure-deflection-curve of a 15 nm thick PS carpet. The response of the polymer carpet is clearly nonlinear and consistent with the

theoretical prediction for the elastic deformation of a thin film in the membrane regime under tension where internal stresses control the mechanical behavior of the layer.[138] The experimental data was fitted with an adequate expression yielding the Young's modulus (E) and the membrane's residual stress at zero pressure.[102] The values of the elastic modulus for PS carpets with various thicknesses using this theoretical model were found to be between 2.0 and 3.0 GPa (Fig. 7b). These moduli are much higher than the values recently reported for highly cross-linked organic/inorganic interpenetrating nanomembranes.[117] These remarkable large values indicate the absence of significant mechanical defects or chinks (cracks, clefts or fissure) within the entire freestanding polymer carpet layer, despite their nanoscale thicknesses down to 10 nm. Fig. 5.18b shows a clear dependency between the Young's modulus and the polymer carpet layer thickness.

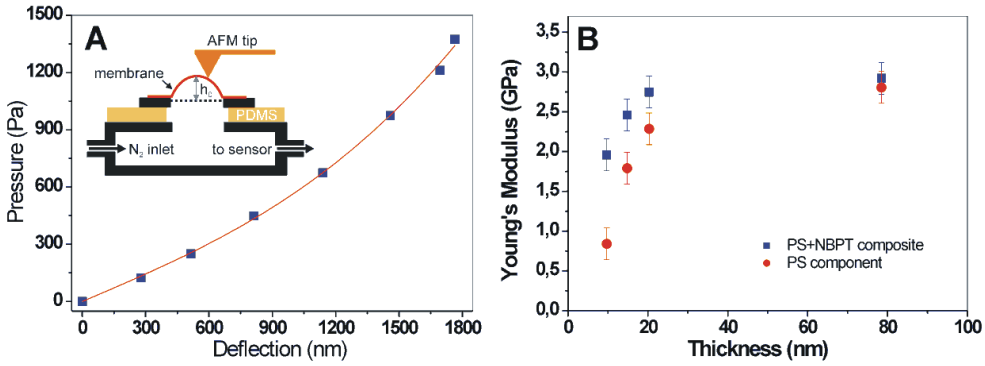

Figure 5.18 Bulging tests with freestanding polymer carpets yield their Young's modulus. (a) The applied pressure as function of the carpet deflection follows equation 1. This allows the extraction of the Young's modulus. The inset shows a scheme of the measurement setup. (b) The Young's modulus of polystyrene carpets of different thicknesses with (blue squares) and without (red circles) the biphenyl monolayer.

It must be pointed out that a polymer carpet is a composite membrane consisting of a cross-linked biphenyl monolayer with a soft polymer brush layer and that the measured elastic modulus is a thickness weighted average between the two compounds.[139] Since the Young's modulus of a single 1 nm thick cross-linked biphenyl monolayer is known to be 12 GPa, the Young's modulus of the PS component could be calculated (red circles in Figure 5.18b). For the thinnest polymer carpet, a modulus of 0.8 GPa was found for the PS brush compound which is far below the PS bulk value of 3.0 GPa.[140] However, thicker PS brush layers reach almost the same Young's modulus as bulk PS. This behaviour corroborates recent findings on PS brushes on solid substrate by Tsukruk et al.[141] Tsukruk et al. also reported that, the Young's modulus of the PS brush layer increased with increasing layer thickness and saturates at the bulk value of polystyrene. It is believed that the level of ordering in the PS chains and the spatial constraints are responsible for the weaker resistance of thin brush layers. Nevertheless, these experiments demonstrate that the micromechanical properties of polymer carpets can be controlled easily by varying the polymer brush layer thickness which can be very precisely controlled over a wide range by varying the SIPGP reaction time as already shown in Fig. 5.13.

5.2.2.3. Summary

The fabrication of self-supporting membranes is reported, membranes with macroscopic lateral dimensions and nanoscale thicknesses consisting of a highly cross-linked monolayer and a soft polymer brush layer, forming a new type of material so-called polymer carpets. These polymer carpets were found to exhibit remarkable and unprecedented properties combining extreme thinness, mechanical and chemical stability, robustness, flexibility and (chemical) sensitivity. Moreover, it was found that the morphology of polymer carpets was driven by interactions between the sensitive brush layer and its environment. By an external chemical stimulus, it was possible to reversibly buckle and unbuckle entire polymer carpet films. This unexpected and to our best knowledge unprecedented reversible conformational change of macroscopic polymer nanomembranes toward an external stimulus was found to be fast and was clearly visible with the naked eye. This intriguing cooperative conformational change could be applied in the development of new types of sensors, displays and micromechanical systems. Furthermore, the two step procedure (electron beam induced SAM crosslinking followed by SIPGP) for the preparation of polymer carpets allows the introduction of multiple chemical functionalities within the layer by varying the monomer or by polymer analogue reactions of grafted polymer chains. Furthermore, the polymer carpet thickness as well as its mechanical properties can be controlled precisely by varying polymerization time. Finally, while we have focussed in this work on the synthesis and characterization of macroscopic and homogeneous

polymer carpets, this two-step approach can potentially be applied in the fabrication of structured, mixed as well as gradient polymer carpets at the micrometer and nanometer scale, since the electron beam induced crosslinking of SAMs by direct writing with a focussed electron beam can be achieved with almost molecular precision. This further expands the variability and scope of this new class of materials and opens a wide variety of potential applications.

5.3. Grafting polymers on structured nanosheets

In the previous section, we have demonstrated the fabrication of fully cross-linked and chemically patterned monolayers on gold substrates generated by electron beam chemical lithography. Such a FCCP monolayer can be lifted off by dissolution of the gold substrate, resulting in a patterned FCCP nanosheet. This FCCP nanosheet can be used as a template for the fabrication of structured, mixed as well as gradient polymer carpets at micrometer and nanometer scale. The patterns generated by EBCL can be achieved with almost molecular precision and thus, offer superior resolution. In this section, the fabrication of structured polymer brushes and freestanding patterned polymer sheets is presented.

5.3.1. non-FCCP sheet

NBPT SAMs were first prepared on gold. The SAMs were structured by EBCL with an electron flood gun through a stencil mask to generate a pattern of cross-linked ABPT and non-cross-linked NBPT areas. Non-FCCP sheets were obtained by directly transferring patterned NBPT SAMs on silicone oxide surface. Subsequent SIPGP was done to grow polymer brushes on chemically patterned nanosheets. Three different experiments were done with identical irradiation parameters using 100 eV electron energy and electron dose of 50mC/cm^2.

In our first experiment, a patterned ABPT nanosheet was immersed in a styrene solution and irradiated for 1 hour. Figure 5.19 shows the optical image of a patterned ABPT nanosheet. Before polymerization, patterns are already visible to the naked eye. This might be due to a big different of reflection between cross-linked ABPT and silicon surfaces that give a higher contrast. After SIPGP of styrene for 1 hour, the thicker PS brushes give an even higher contrast and each single PS dot is even observable (Fig. 5.19b). This indicates that a high grafting density of PS brushes was achieved.

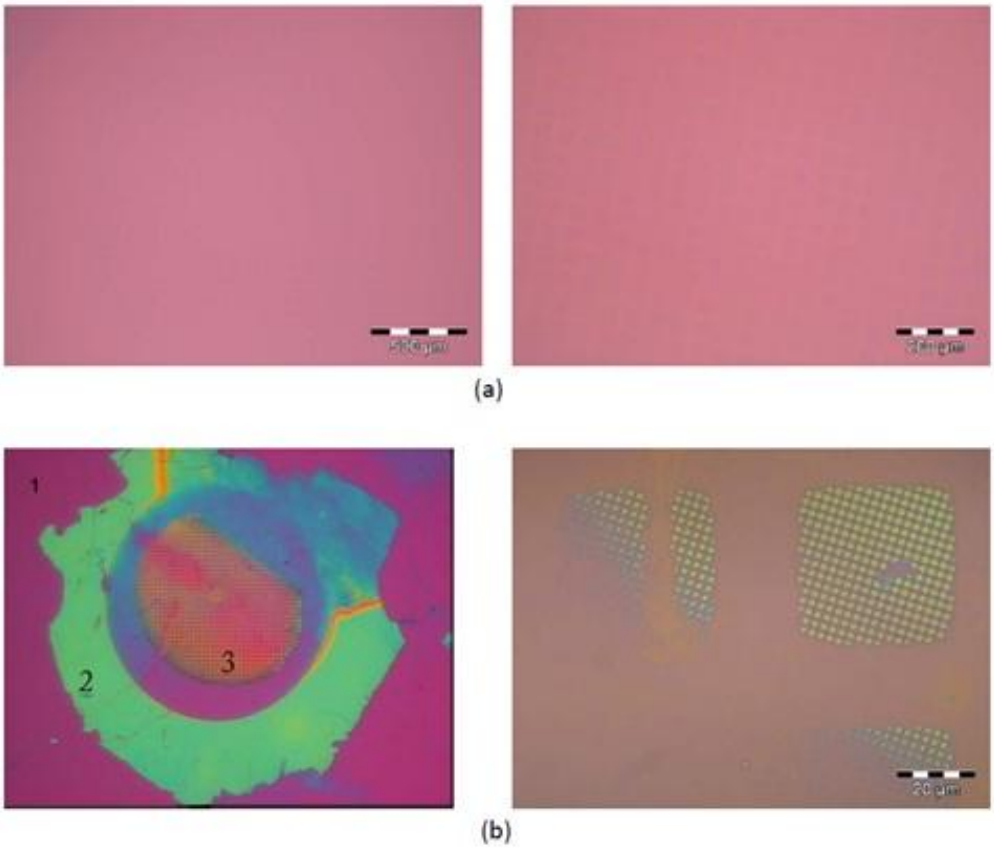

Figure 5.19 Optical images of a non-FCCP nanosheet (a) before, and (b) after SIPGP of styrene for 1 h. Structures are visible by the naked eye.

As pointed before, SIPGP can only occur in cross-linked ABPT areas: the monomer (styrene)[100, 126, 127] absorbs a photon and acts as photosensitizer to activate functionality of a surface by hydrogen abstraction. The radical formed on the amino groups initiates the free radical polymerization. Polymer brushes were selectively grafted on patterned areas. As apparent from figure 5.20, the height of PS brush obtained by SIPGP is 162nm.

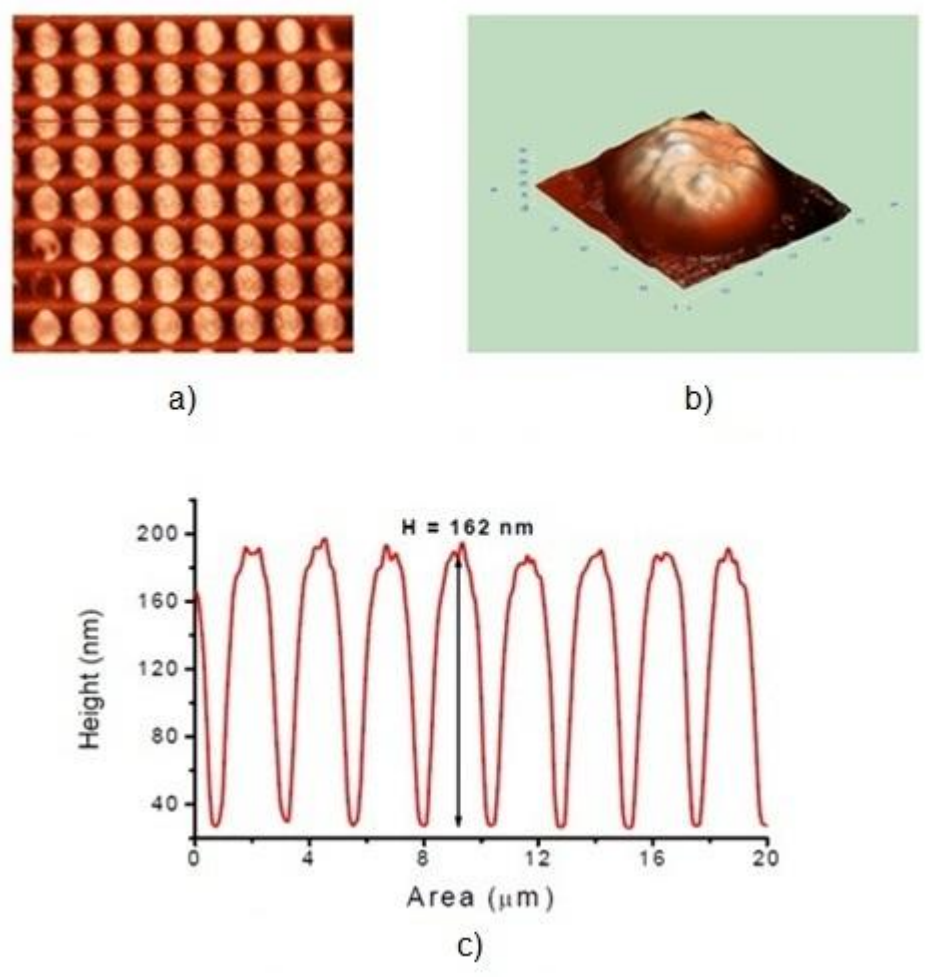

Figure 5.20 a) AFM scan area of 20 x 20 μm^2 of PS brushes grafted on patterned nanosheet; b. 3D representation of single PS dot; c) line profile of PS dots from (a).

For a second experiment, methylmetacrylate was used as the monomer. The patterned ABPT sheet was submerged in a MMA solution and irradiated for 30 minutes.

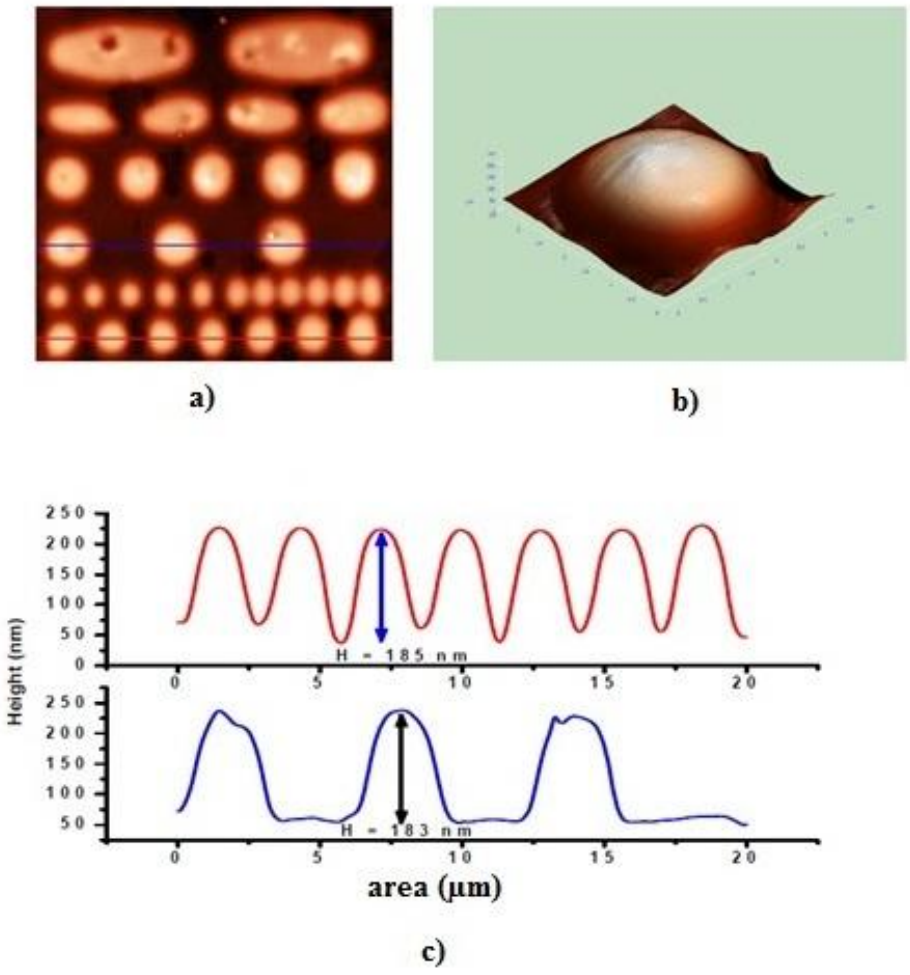

Figure 5.21 a) AFM image of 20 x 20 µm^2 PMMA grafted on patterned nanosheet. b) 3D representation of single PMMA dot shows a smooth shape, indicating homogenous electron irradiation as well as polymerization. c) Line profiles from two different areas.

The sample was then scanned with AFM. A polymer layer of 185 nm was measured. A line profile from different area gives a similar value, indicating homogeneity of the PMMA brush.

In the last experiment, 4-vinyl-pyridine was used. A layer of P4VP brushes of 60 nm was obtained after 1 h polymerization, as shown by figure 5.22.

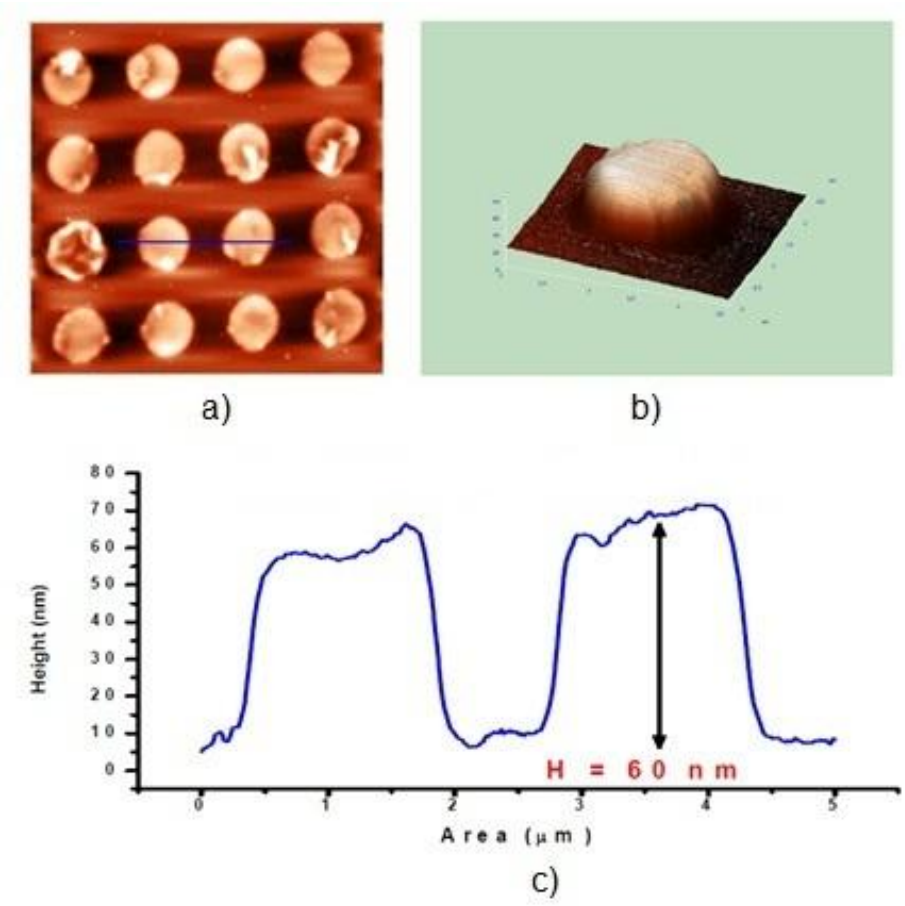

Figure 5.22 a) AFM scans of 10x10 µm^2 area of structured P4VP brushes, b) 3D representation of single P4VP dot, and c) line profile of P4VP dots.

The result on the thickness measurements is shown I Table 5.2; it shows that PMMA brushes are thicker than PS brushes. This can be explained as MMA has a higher growth rate (k_g) than styrene[140], whereas 4-vinyl-pyridine has the lowest k_g. Steenackers et al. have reported the value of growth rate for several monomers.[20]

Table 5.2. Thickness of different polymer layer obtained by SIPGP.

Monomer	Polymerization time	Thickness
Styrene	1 hour	162 nm
MMA	30 minutes	185 nm
4-Vinyl-Pyridine	1 hour	60 nm

As shown, all single polymer brush dots have a regular smooth shape. This indicates that homogenous electron irradiation during patterning the SAMs by EBCL was achieved. As a result, patterned polymer brushes were fabricated at superior resolution.

5.3.2. Grafting polymers on FCCP nanosheet

As presented in section 5.1.3, patterned FCCP nanosheet, both positive and negative, can be fabricated from FCCP monolayers[142] after dissolution of the gold substrate. These FCCP nanosheets can be used as a template for the fabrication of well defined, structured polymer brushes. Since the patterned nanosheets are fully cross-linked, it will be possible to obtain freestanding patterned polymer brushes.

Both positive and negative FCCP nanosheets were fabricated using the procedure described in sections 5.1 and 5.3. Polymerization for both patterned samples was performed under identical conditions. Both samples were immersed in a solution of styrene and irradiated with UV-light for 30 minutes. A mask with circular

opening with diameter of 2.4 µm (quantifoil mask R1.2/1.3) was used to generate patterns. For positive FCCP nanosheet, as shown in fig. 5.23 , patterns are cABPT while the adjacent areas are cBPT.

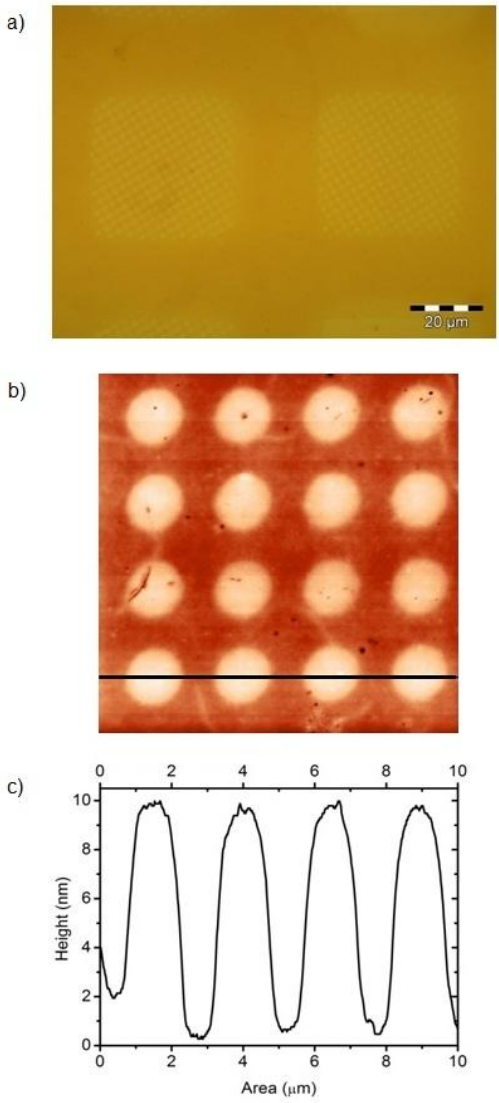

Figure 5.23 Positive FCCP nanosheet after SIPGP of styrene for 30 minutes. a) optical image, b) 10 x 10 µm AFM image and c) line profile. Amino terminated areas (circular patterns) appear higher ~10 nm. This indicates that styrene has a tendency to couple to amino group.

AFM measurement at the edge of sample shows that PS brushes were grafted not only on cABPT pattern areas, but also on cBPT. cBPT can also provide hydrogen radical abstraction. Thus, the radical on cBPT can also initiate free radical polymerization. However, cBPT has a R-H bond dissociation energy (BDE) of 111 kcal/mol compared to only 89.3 kcal/mol for cABPT[20]. Bond dissociation energy is the amount of energy of the surface which has to be overcome by the potential energy of the photoactivated monomer to enable photopolymerization to take place. The lower the BDE of the surface, the easier it is for a monomer to form radicals on that surface and initiate polymerization.

If the potential energy of the photoactivated monomer is lower than surface BDE, no polymerization occurs.[58] Since cABPT has a lower BDE than cBPT, styrene is more favorable to couple to amino groups. That is why a height increase of amino terminated areas was still observed. As seen in figure 5.23, pattern cABPT areas appear higher. The measured height difference between cABPT and cBPT after polymerization is ~10 nm.

A Negative pattern FCCP nanosheet has been also used as template for polymerization. As expected, after polymerization of styrene for 30 minutes, the adjacent areas -which are amino terminated groups- appear higher than the circular patterns of cBPT, giving a depth profile. The AFM image in figure 5.24 shows that the measured height difference, or the depth, between cABPT and cBPT is ~12 nm. This result is in agreement with a positive pattern.

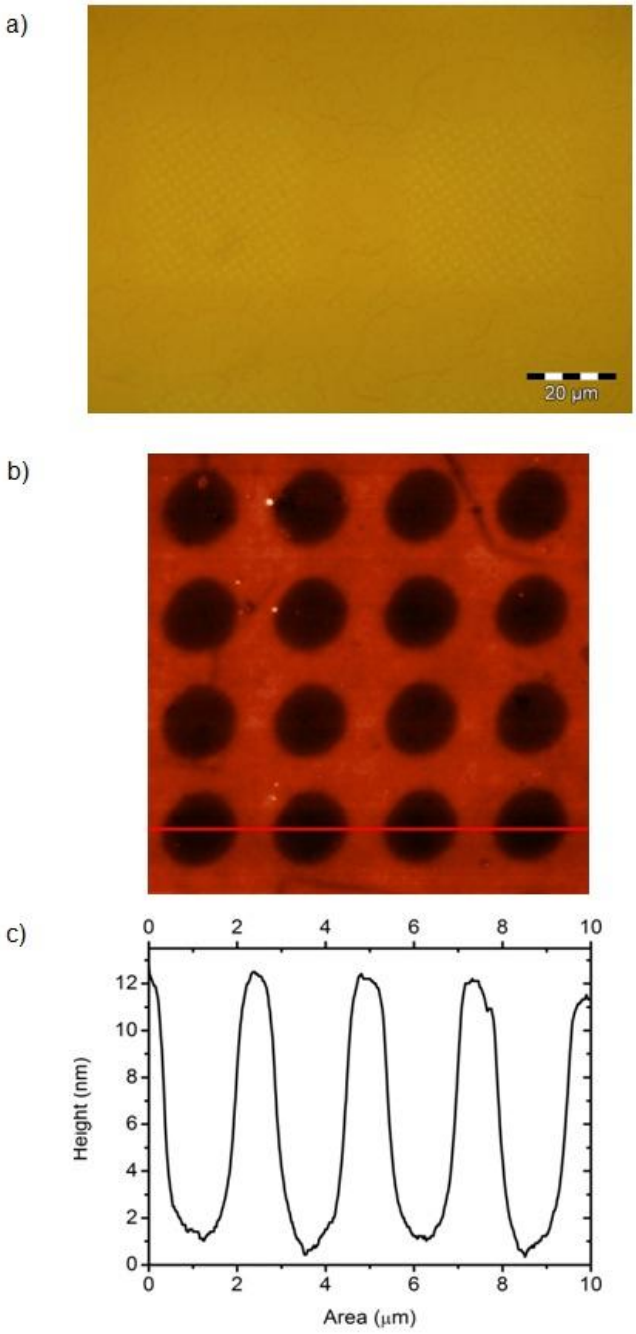

Figure 5.24 Negative FCCP nanosheet after SIPGP of styrene for 30 minutes. a) Optical image, b) AFM image of 10 x 10 µm scan area, and c) line profile. Amino groups appear ~12 nm higher than pattern cBPT, giving a depth profile.

5.3.3. Freestanding patterned polymer sheet

For fabrication of freestanding patterned polymer brushes, both positive and negative patterned FCCP nanosheets were used as templates for polymerization. After dissolution of the sacrificial layer, the patterned polymer sheet can be transferred for example to a TEM grid with hexagonal holes or silicon windows. For many occasion, no problem is encountered while transferring a negative patterned polymer sheet on TEM grid, whilst positive patterned sheets were always broken. The negative pattern polymer sheet was found to be more stable than the positive one. This may be explained as follows: in a negative pattern, PS brushes are grafted on the adjacent regions which cover more areas compared to the pattern areas. The thickness of polymer brushes compensates for the thinness of pattern areas. This enhances the mechanical stability of the layer. In a positive pattern, PS brushes are only on pattern areas, whilst the adjacent regions are thinner, thus, the positive patterned brush is more fragile. This likely explains why the positive patterned brushes are often broken during transfer to TEM grid. Figure 5.25, shows optical images of freestanding negative patterned polystyrene brushes on a TEM grid with hexagonal openings with a diameter of ~50 µm. This sample was obtained from dissolution of the gold substrate of the sample shown in figure 5.24. The patterned layer was stable enough to cover a TEM grid up to several millimeters. The optical images were taken from the same sample with different resolution. No optical enhancement was performed to obtain the high resolution image of the polymer layer.

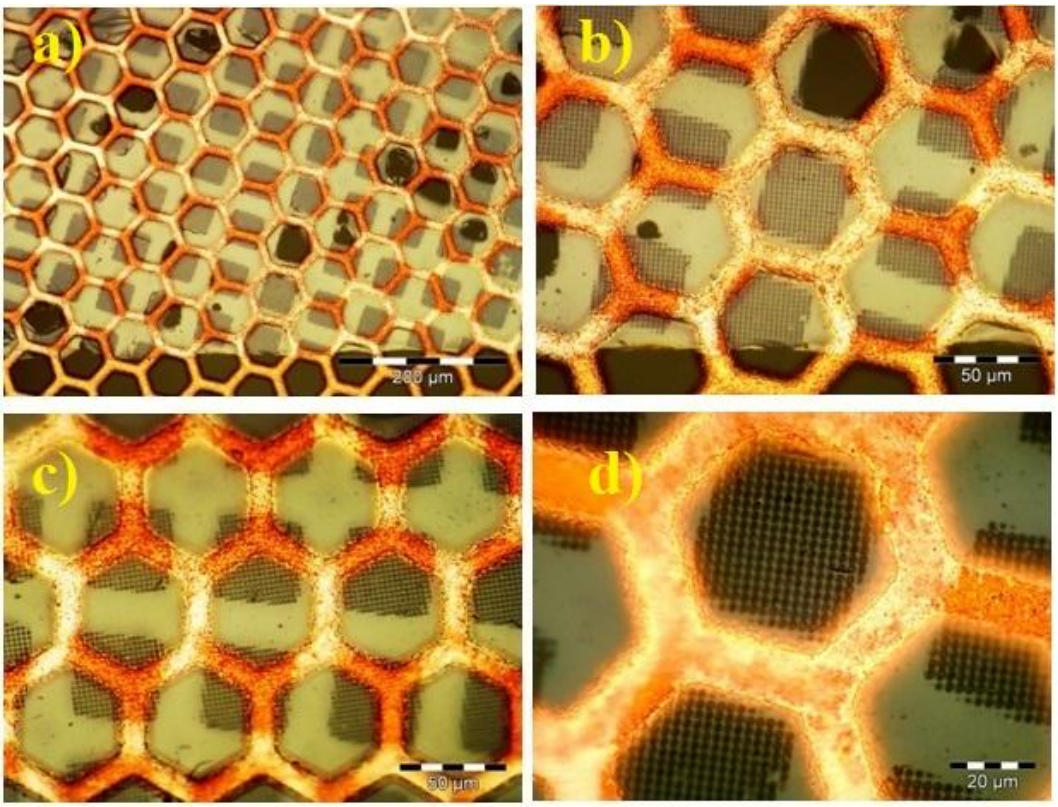

Figure 5.25 Optical images of freestanding negative patterned nanosheet for the corresponding sample shown in fig. 5.24.

Optical images show a sharp contrast and a good resolution between polymer brushes on adjacent and pattern areas. Patterns are also clearly visible. The black dots refer to the depth profiles or the holes created by the height difference between the adjacent cABPT and the pattern cBPT. Thus, the optical image reflects and is in agreement with AFM results (AFM shows that a negative pattern polymer sheet has a depth profile, indicating that the pattern cBPT is lower than the adjacent areas).

Another attempt to fabricate freestanding positive patterned polymer brushes was done. A positive patterned FCC nanosheet was immersed in a solution of styrene for 4 hours. The longer polymerization time was considered, expecting that thicker positive patterned brushes would be obtained. To our surprise, a negative-like pattern was observed.

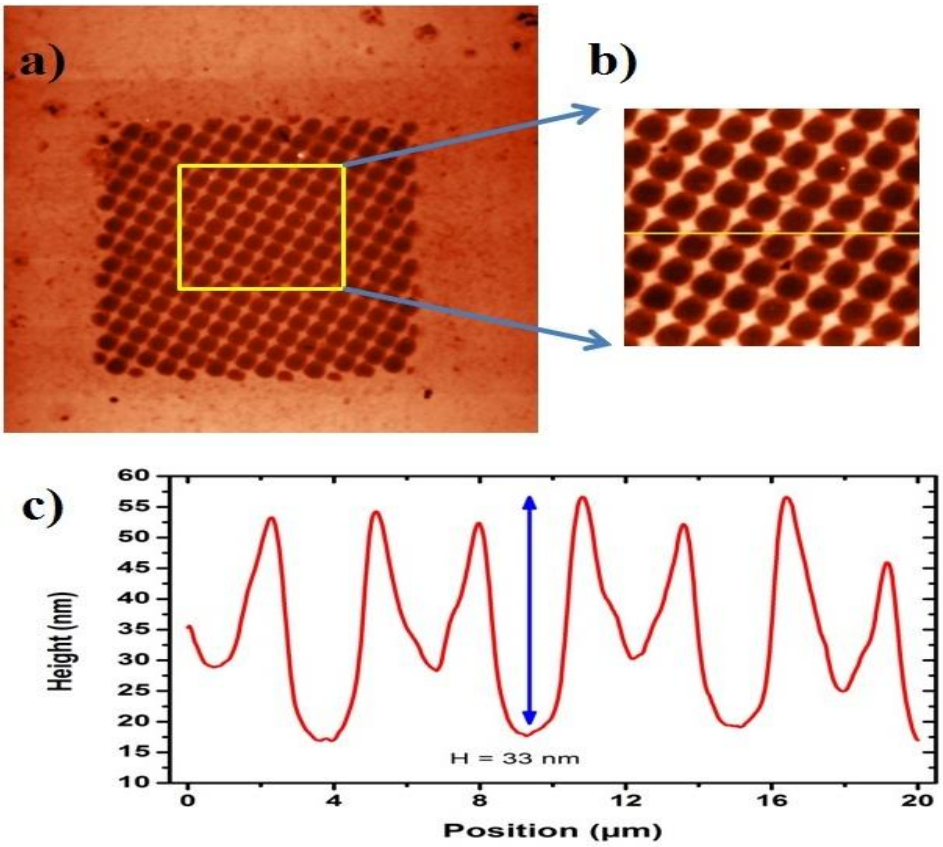

Figure 5.26 AFM image of positive pattern after 4 hours polymerization with styrene. Instead of positive brush pattern, negative patterned brush obtained, with the circular patterns appear 33 nm lower.

On a positive pattern, patterns are amino terminal groups while the adjacent areas are cBPT. However, our result showed differently, the adjacent areas appear high-

er than the dot patterns, creating hole structures where the depth of a single hole is ~33 nm. It is difficult to find a direct explanation. An AFM measurement made at the edge of the sample shows a thickness difference of ~53 nm between the adjacent region and the bare silicon area, as shown in figure 5.27. Since the depth of the hole is ~33 nm, it gives a thickness difference of 20 nm between the amino part and bare silicon. This means PS brushes of 20 nm was grafted on amino areas. In short, during the 4 hour polymerization, styrene was first coupled to pattern areas. When saturation was reached, styrene covered on the whole nanosheet. This might be a possible explanation for the negative pattern-like PS brushes we obtained on a positive patterned sheet. Further investigation needs to be carried out to corroborate this explanation.

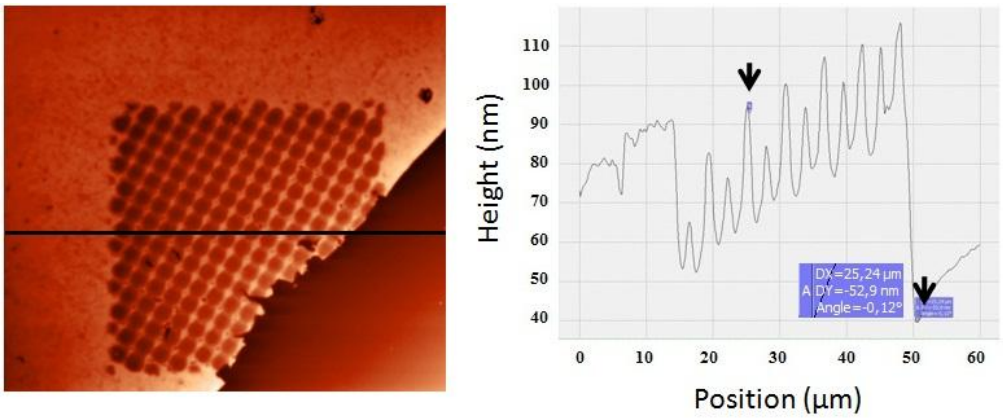

Figure 5.27 AFM scans the edge sample. A height difference of ~53 nm was obtained between the adjacent area and the bare silicon substrate.

A freestanding patterned polymer sheet was obtained by transferring the sample onto a TEM grid. The thicker PS layer has an increased mechanical stability. A TEM grid with bigger hexagonal holes with a diameter of 125 µm was used. The

optical images of the freestanding polymer sheet are shown in figure 5.28. A sharp contrast was obtained. In agreement with AFM, the patterns appear darker higher. Due to the high contrast, a single dot pattern is also observable.

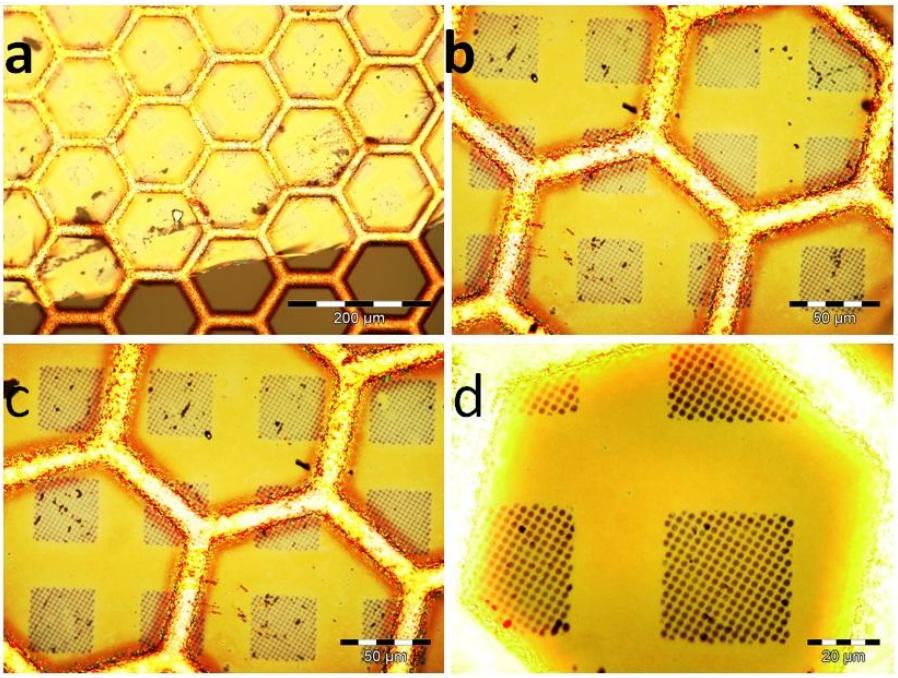

Figure 5.28 Optical images of different resolution of freestanding patterned PS brushes.

5.3.4. Summary

We have shown the fabrication of freestanding patterned polymer brushes by combining patterned FCCP nanosheet and SIPGP. The polymer layer is mechanically stable enough to enable transfer to the larger opening of a TEM grid. A higher pattern resolution and almost defect-free on large areas of freestanding sheet have achieved.

6. Conclusions and Outlook

This work deals with the preparation and fabrication of freestanding polymer brushes both homogenous and patterned.

A fully cross-linked and chemically patterned monolayer has been fabricated by means of EBCL and an exchange process between two aromatic molecules. EBCL is a powerful patterning tool which offers high selectivity, flexibility and high resolution. An electron beam induces crosslinking in the monolayer. This enhances the mechanical stability of the monolayer; hence, it is possible to release the monolayer by dissolution of its substrate. This results in a flat and two dimensionally extended layer which is better known as a nanosheet. Both homogenous and patterned nanosheets can be fabricated. Nanosheets are extremely stable, mechanically and thermally. This makes them an excellent candidate for a template for polymerization.

To fabricate freestanding polymer brushes, nanosheets combined with surface initiated polymerization photografting photopolymerization (SIPGP) have been utilized. The SIPGP technique offers a simple procedure for preparing polymer brushes. In SIPGP, a SAM-modification step for the preparation of a surface-bonded initiator is not needed. Hence, a tedious, tricky step in the preparation of polymer brushes can be avoided and the polymerization process becomes simplified. The polymer grafts exhibit remarkable properties (optical, wetting) combin-

ing extreme thinness, mechanical stability, robustness, flexibility and unprecedented chemical sensitivity.

Freestanding patterned polymer brushes were also fabricated by subsequent SIPGP on a FCCP nanosheet. Patterned brushes with a high resolution as well as with a large almost defect-free area can be achieved.

Freestanding polymers respond faster as a result of the isolation from the supporting substrate. This will make them excellent materials for surface-based sensors, nanoactuators, MEMs and for cell adhesion studies. Negative patterned polymer brushes can be used for particle-based diagnostic in microfluidic systems. The hole sites can be used as a dock site to capture and or release particles.

The work presented in this thesis offers a simple route for polymerization and may lead to a new technology platform in the fabrication of freestanding polymer brushes both homogenous and patterned. The results may play important role in the development of new surface-based technology. Furthermore, freestanding polymers may open a new perspective in understanding two dimensional polymeric systems.

References

[1] A. Ulman, *Chem. Rev*., **1996**, 96, 1533–1554.

[2] F. Schreiber, *J. Phys. Condens. Matter*, **2004**, 16, R881–R900.

[3] F. Schreiber, *Structure and Growth of Self-Assembling Monolayers, Progress in Surface Science* 65, **2000**, 151.

[4] C. Love, L. A. Estroff, J. K. Kriebel, R. G. Nuzzo, G. M. Whitesides, *Chem. Rev.*, **2005**, 105, 1103–1169.

[5] Y. Liu, L. Mu, B. Liu, J. Kong, *Chem. Eur. J*., **2005**, 11, 2622-2631.

[6] S. Edmondson, V. L. Osborne, W. T. S. Huck, *Chem. Soc. Rev*., **2004**, 33, 14-22.

[7] P. Uhlmann, H. Merlitz, J. Sommer, M. Stamm, *Macromol. Rapid. Commun.*, **2009**, 30, 732-740.

[8] R. C. Advincula, W. J. Brittain, K. C. Caster, J. Ruehe, *Polymer Brushes: Synthesis, Characterization, Applications,* Wiley-VCH Verlag GmbH & Co KGaA, Weinheim, Germany, **2004**.

[9] F. Zhou, Z. Zheng, B. Yu, Weimin, W. S. Huck, *J. Am. Chem. Soc*., **2006**, 128, 16253-16258.

[10] M. Woodson, J. Liu, J. *Phys. Chem. Chem. Phys.,* **2007**, *9*, 207.

[11] H. B. Akkerman, P. W. M. Blom, D. M. de Leeuw, B. de Boer, *Nature,* **2006**, *441*, 69.

[12] K. S Chen, I. K. Lin; F. H. Ko,. *J. Micromech. Microeng.*, **2005**, 15, 1894.

[13] S. Valkama, *Nat. Mat*., **2004**, 3, 872-876.

[14] M. Champbell, D. N. Sharp, M. T. Harrison, R. G. Denning, A. Tuberfield, *Nature*, **2000**, 404, 53-56.

[15] Q. J. Niu, J. M. J. Frechet, *Angew. Chem. Int. Ed*., **1998,** 37, 667.

[16] H. G. Craighead, *Science,* **2000**, *290*, 1532.

[17] Y. Xia, G. Whitesides, *Angew. Chem. Int. Ed*., **1998**, 37, 550-575.

[18] R. K. Smith, P. A. Lewis, P. S. Weiss, *Progress in Surface Science*, **2004**, 75, 1-68.

[19] G. G. Baralia, A. Pallandre, B. Nysten, A. M. Jonas, *Nanotechnology*, **2006**, 17, 1160-1165.

[20] M. Steenackers, Micro- and Nanostructured Polymer Graft, PhD Thesis, **2007**, TU München, Germany.

[21] C. Y. Jiang, V. V. Tsukruk, *Adv. Mater*., **2006**, 18, 829.

[22] V. V. Tsukruk, *Adv. Mater*., **2001**, 13, 95.

[23] W. T. Huck, *materials today*, **2008**, 11, 24-32.

[24] M. Mitsuishi, J. Matsui, T. Miyashita, *J. Mater. Chem.*, **2009**, 19, 325-329.

[25] C. Jiang, S. Markutsya, Y. Pikus, V. V. Tsukruk, *Nat. Mat*., **2004**, 3, 721-728.

[26] H. Endo, M. Mitsuishi, T. Miyashita, *J. Mater. Chem*., **2008**, 18, 1302-1308.

[27] S. T. Milner, *Science*, **1991**, 251, 905.

[28] A. Halperin, M. Tirrell, T. P. Lodge, *Adv. Polym. Sci.*, **1992**, 100, 31.

[29] I. Szleofer, M. A. Carignano, *Adv. Chem. Phys.*, **1996**, 94, 165.

[30] G. Reiter, P. Auroy, L. Auvray, *Macromolecules*, **1996**, 29, 2150.

[31] G. Reiter, R. Khanna, *Langmuir*, **2000**, 16,6351.

[32] J. F. Douglas, M. S. Kent, S. K. Satija, A. Karim, *Polymer Brushes: Structure and Dynamics.* In: Buschow, K. H. J. (Ed) Encyclopedia of Materials: Science and Technology, Elsevier, Amsterdam, **2001**.

[33] M. Steenackers, A. Küller, N. Ballav, M. Zharnikov, M. Grunze, R. Jordan, *Small*, **2007**, *3*, 1764.

[34] G. Tovar, S. Paul, W. Knoll, O. Prucker, J. Rühe, *Supramol. Sci*., **1995**, 2, 89–98.

[35] R. Jordan, A. Ulman, *J. Am. Chem. Soc*., **1998**, 120, 243–247.

[36] S. Roux; S. Demoustier-Champagne, *J. Polym. Sci., **2003**, A* 41, 1347.

[37] C. Yoshikawa, A. Goto, Y. Tsujii, T. Fukuda, K. Yamamoto, A. Kishida, *Macromolecules,* **2005**, 38,604.

[38] W. H. Yu, E. T. Kang, K. G. Neoh, *Langmuir*, **2005**, 21, 450.

[39] E. T. Kang, Y. Zhang, *Adv. Mater.,* **2000**, 12, 1481.

[40] Y. Chen, E. T. Kang, G. K. Neoh, K. L. Tan, *J. Phys. Chem.,* **2000**, *B* 104, 9171.

[41] D. O. H. Teare, D. C. Barwic, W. C. E. Garrod Schofield, R. P. Ward, L. J. Badval, J. P. S., *Langmuir*, **2005**, *21*, 11425.

[42] C. Padeste, P. Farquet, C. Potzner, H. H. Solak, *J. Biomater. Sci. Polymer Edn*., **2006**, *17*, 1285.

[43] O. Prucker, J. Rühe, *Macromolecules*, **1998**, 31, 602–613.

[44] O. Prucker, J. Rühe, *Macromolecules*, **1998**, 31, 592–601.

[45] R. Jordan, A. Ulman, *J. Am. Chem. Soc.*, **1998**, *120*, 243. **b)** R. Jordan, N. West, A. Ulman, Y. M. Chou, O. Nuyken, *Macromolecules*, **2001**, *34*, 1606. **c)** M. D. K. Ingall, C. H. Honeyman, J. V.Mercure, P. A. Bianconi R. R. Kunz, *J. Am. Chem. Soc*., **1999**, 121, 3607–3613.

[46] R. Jordan, A. Ulman, J.F. Kang, M.H. Rafailovich, J. Sokolov*; J. Am. Chem. Soc.*, **1999,** 121, 1016-1022.

[47] N. Y. Kim, N. L. Jeon, I. S. Choi, S. Takami, Y. Harada, K. R. Finnie, G. S. Girolami, R. G. Nuzzo, G. M. Whitesides, P. E. Laibinis, *Macromolecules*, **2000**, *33*, 2793.

[48] R. Laible, K. Hamann, *Adv. Coll. Interface Sci.*, **1980**, *13*, 65.

[49] J. Li, X. Chen, Y.-C. Chang, *Langmuir*, **2005**, 21, 9562 .

[50] K. Matyjaszewski, P. J. Miller, N. Shukla, B. Immaraporn, A. Gelman, B. B. Luokala, T. M. Siclovan, G. Kickelbick, T. Vallant, H. Hoffmann, T. Pakula, *Macromolecules*, **1999**, 32, 8716.

[51] A. Ramakrishnan, D. Dhamodharan, J. Rühe, *J. Polym. Sci. A*, **2006**, 44, 1758.

[52] K. Yamamoto, H. Tanaka, M. Sakaguchi, S. Shimada, *Polymer*, **2003,** 44**,** 7661.

[53] Y.-P. Wan, X.-W. Pei, X.-Y. He, Z. Q. Lei, *Eur. Polymer J.*, **2005**, 41, 737.

[54] C. Yoshikawa, A. Goto, Y. Tsujii, T. Fukuda, K. Yamamoto, A. Kishida, *Macromolecules*, **2005**, 38, 4604.

[55] W. T. Yang, B. Rånby, *J. Appl. Polym. Sci.,* **1996**, *62*, 533.

[56] W. T. Yang, B. Rånby, *Polym. Bull.,* **1996**, *37*, 89.

[57] a. S. J. Li, C. G. Li, T. Li, J. J. Cheng: *"Polymer Photochemistry principles andApplications", 1st edition, Fudan University Press, Shanghai.* **1993**, 110; b. J. P. Deng, W. T. Yang, B. Rånby, B. *Macromol. Rapid Commun.,* **2001**, *22*, 535.

[58] H. Wang, H. R. Brown, *Macromol. Rapid Commun.,* **2004**, *25*, 1095.

[59] W. H. Fang, R. Z. Liu, *J. Am. Chem. Soc.,* **2000**, *122*, 10886.

[60] J. M. Hollas, T. J. Ridley, *Mol. Spectrosc.,* **1981**, *89*, 232.

[61] J. Wan, H. Nakatsuji, *Chem. Phys.,* **2004**, *302,* 125.

[62] D. J. Dyer, J. Feng, R. Schmidt, V. N. Wong, T. Thao, Y. Yagci, *Macromolecules*, **2004**, *37*, 7072.

[63] M. Motornov, R. Sheparovych, E. Katz, S. Minko, *ACS Nano*, **2008**, 2, 41.

[64] S. H. Lee, H. E. Jeong, M. C. Park, J. Y. Hur, H. S. Cho, S. H. Park, K. Y. Suh, *Adv. Mater*., **2008**, 20, 788.

[65] H. K. Wu, T. W. Odom, G. M. Whitesides, *Anal. Chem*., **2002**, 74, 3267.

[66]] R. Ducker, A. Garcia, J. Zhang, T. Chen, S. Zauscher, *Soft Matter,* **2008**, 4, 1774.

[67] A. S. Blawas, W. M. Reichert, *Biomaterials*, **1998**, 19, 595–609.

[68] R. C. Bailey, J. T. Hupp, *Anal. Chem*., **2003**, 75, 2392.

[69] C. T. Black, R. Ruiz, G. Breyta, J. Y. Cheng, M. E. Colburn, K. W. Guarini, H. C. Kim, Y. Zhang, *IBM J. Res. Dev*., **2007**, 51, 605-633.

[70] T. Chen, J. Zhang, D. P. Chang, A. Garcia, S. Zauscher, *Adv. Mater*., **2009**, 21, 1825-1829.

[71] M. Lahav, M. Narovlyansky, A.Winkleman, R. Perez-Castillejos, E. A. Weiss, G. M. Whitesides, *Adv. Mater*., **2006**, 18, 3174.

[72] A. Jahn, W. N. Vreeland, M. Gaitan, L. E. Locascio, *J. Am. Chem. Soc*., **2004**, 126, 2674.

[73] S. Jeon, V. Malyarchuk, J. O. White, J. A. Rogers, *Nano Lett*., **2005**, 5, 1351.

[74] M. Mrksich, G. M. Whitesides, *Trends Biotechnol*., **1995**, 13, 228–235.

[75] S.A. Letsche, A. M. Steinbach, M. Pluntke, O. Marti, A. Ignatius, D. Volkmer, *Frontiers of Materials Science in China*, Volume 3, Issue 2, **2009**, First Page 132.

[76] M. Hirtz, M. K. Brinks, S. Miele, A. Studer, H. Fuch, L. Chi, *Small*, **2009**, 5, no. 8, 919-923.

[77] M. Théry, V. Racine, A. Pepin, M. Piel, Y. Chen, J. B. Sibarita, M. Bornens, *Nature Cell Biol*., **2005**, 7, 947–953.

[78] M. Théry, V. Racine, M. Piel, A. Pépin, A. Dimitrov, Y. Chen, J. Baptiste-Sibarita, M. Bornens, *Proc. Natl. Acad. Sci., USA*, **2006**, 103, 19771–19776.

[79] S. J. Hollister, *Nature Mater*., **2005**, 4, 518–524.

[80] O. Prucker, M. Schimmel, G. Tovar, J. Rühe, *Adv. Mat*., **1998**, 10, 1073.

[81]. U. Schmelmer, A. Paul, A. Küller, M. Steenackers, A. Ulman, M. Grunze, A. Gölzhäuser, R. Jordan, *Small*, **2007**, 3, no. 3, 459 – 465.

[82] M. Steenackers, A. Küller, N. Ballav, M. Zharnikov, M. Grunze, R. Jordan, *Small*, **2007**, 3, no. 10, 1764 – 1773.

[83] U. Schmelmer, R. Jordan, W. Geyer, W. Eck, A. Gölzhäuser, M. Grunze, A. Ulman, *Angew. Chem. Int. Ed*., **2003**, 42, 559.

[84] M. Kaholek, W.-K. Lee, B. LaMattina, K. C. Caster, S. Zauscher, *Nano Lett.*, **2004**, 4, 373.

[85] X. G. Liu, S. W. Guo, C. A. Mirkin, *Angew. Chem. Int. Ed.*, **2003**, 42, 4785.

[86] B. W. Maynor, S. F. Filocamo, M. W. Grinstaff, J. Liu, *J. Am. Chem. Soc.*, **2002**, 124, 522.

[87] Y. Okawa, M. Aono, *Nature,* **2001**, 409, 683.

[88]. Y. N. Xia, G. M. Whitesides, *Angew. Chem. Int. Ed.*, **1998**, 37, 551.

[89] D. M. Jones, W. T. S. Huck, *Adv. Mater.*, **2001**, 13, 1256.

[90] K. C. A. Smith, C. W. Oatley, C. W. *J. Appl. Phys.*, **1995**, *6*, 391.

[91] W. Geyer, V. Stadler, W. Eck, M. Zharnikov, A. Gölzhäuser, M. Grunze, *Appl. Phys. Lett.*, **1999**, 75, 2401.

[92] W. Eck, V. Stadler, W. Geyer, M. Zharnikov, A. Gölzhauser, M. Grunze, *Adv. Mater*., **2000**, 12 (11), 805.

[93] A. Gölzhauser, W. Geyer, V. Stadler, W. Eck, M. Grunze, K. Edinger, T. Weimann, P. Hinze, *J. Vac. Sci. B*, **2000**, 18(6), 3414.

[94] A. Gölzhauser, W. Eck, V. Stadler, T. Weimann, P. Hinze, M. Grunze, *Adv. Mater*., **2001**, 13 (11), 806.

[95] W. Geyer, V. Stadler, W. Eck, A. Gölzhäuser, M. Grunze, M. Sauer, T. Weimann, P. Hinze, *J. Vac. Sci. B*, **2001**, 19(6), 2732.

[96] W. Eck, A. Küller, M. Grunze, B. Völkel, A. Gölzhäuser, *Adv. Mater.*, **2005**, 17, 2583.

[97] O. Nuyken, R. Weidner, *Adv. Polym. Sci.*, **1986**, 37, 147.

[98] O. Prucker, J. Habicht, I.-J. Park, J. Rühe, *Mater. Sci. Eng. C,* **1999**, 8-9, 291.

[99] N. Fery, R. Hoene, K. Hamann, *Angew. Chem.*, **1972**, 84 359.

[100] M. Steenackers, A. Küller, S. Stoycheva, M. Grunze, R. Jordan, *Langmuir*, **2009**, 25, 2225.

[101] C.T. Nottbohm, A. Beyer, A. S. Sologubenko, I. Ennen, A Hütten, H. Rösner, W. Eck, J. Mayer, A. Gölzhäuser, *Ultramicroscopy*, **2008**, 108, 885– 892.

[102] A. Turchanin, A. Beyer, C. T. Nottbohm, X. Zhang, R. Stosch, A. Sologubenko, J. Mayer, P. Hinze,T. Weimann, A. Gölzhäuseruser. *Adv. Mater*., **2009**, 21, 1233–1237.

[103] S. Liao, Y. Shnidman, A. Ulman, *J. Am. Chem. Soc*., **2000**, 122, 3688–3694.

[104] A. Turchanin, A. Tinazli, M. El-Desawy, H. Großmann, M. Schnietz, H. H. Solak, R. Tampé, A. Gölzhäuser, *Adv. Mater*., **2008**, 20, 471–477.

[105] C. Casiraghi, A. Hartschuh, E. Lidorikis, H. Qian, H. Harutyunyan, T. Gokus, K. S. Novoselov, A. C. Ferrari, *Nano Letters*, **2007**, 7(9), 2711-2717.

[106] M. B. Shiflett, H. C. Foley, *Science*, **1999**, 285, 1902-1905.

[107] A. Rogalski, Infrared detectors: status and trends, *Progr. Quant. Electron.*, **2003**, 27, 59-210.

[108] X. Wang, C. Drew, S. Lee, K. Senecal, J. Kumar, L. Sarnuelson, Electrospun Nanofibrous Membranes for Highly Sensitive Optical Sensors, *Nano Lett.*, **2002**, 2, 1273-1275.

[109] W. T. Huck, A. D. Stroock, G. M. Whitesides, A Novel Catalytic System for the Mannich-Type Reaction of Silyl Enolates: Stereoselective Synthesis of Aminoketones,.*Angew. Chem. Int. Ed*., **2000,** 39, 1958-1960.

[110] F. Mallwitz, A. Laschewsky, Direct Access to Stable, Freestanding Polymer Membranes by Layer-by-Layer Assembly of Polyelectrolytes, *Adv. Mater.*, **2005** 17, 1296-1299.

[111] F. Mallwitz, W. A. Goedel, Influence of Structural and Rotational Isomerism on the Triplet Blinking of Individual Dendrimer Molecules, *Angew. Chem. Int. Ed.*, **2001**, 40, 4645-4648.

[112] C. Nardin, M. Winterhalter, W. Meier, Giant Free-Standing ABA Triblock Copolymer Membranes, *Langmuir*, **2000**, 16, 7708-7712.

[113] J. Mattsson, J. A. Forrest, L. Borjesson, Quantifying glass transition behavior in ultrathin free-standing polymer films, *Phys. Rev. E*, **2000**, 62, 5187-5200.

[114] C. Jiang, S. Markutsya, Y. Pikus, V. V. Tsukruk, Freely suspended nanocomposite membranes as highly sensitive sensors, *Nat. Mater.*, **2004,** 3, 721-728.

[115] H. Ko, C. Jiang, H. Shulda, V. V. Tsukruk, Carbon Nanotube Arrays Encapsulated into Freely Suspended Flexible Films, *Chem. Mater.*, **2005**, 17, 2490-2493.

[116] H. Watanabe, R. Vendamme, T. Kunitake, Development of Fabrication of Giant Nanomembranes, *Bull. Chem. Soc. Jpn.*, **2007**, 80, 433-440.

[117] R. Vendamme, S. Y. Onoue, A. Nakao, T. Kunitake, Robust free-standing nanomembranes of organic/inorganic interpenetrating networks, *Nat. Mater.*, **2006**, 5, 494-501.

[118] E. T. Carlen, M. S. Winberg, C. E. Dubé, A. M. Zapata, J. T. Borenstein, Micromachined silicon plates for sensing molecular interactions, *Appl. Phys. Lett.*, **2006**, 89, 173123.

[119] C. Stampfer, T. Helbling, D. Obergfell, B. Scho1berle, M. K. Tripp, A. Jungen, S. Roth, V. M. Bright, C. Hierold, Fabrication of Single-Walled Carbon-Nanotube-Based Pressure Sensors, *Nano Lett.*, **2006**, 6, 233-237.

[120] Z. Tang, N. A. Kotov, S. Magonov, B. Ozturk, Nanostructured artificial nacre, *Nat. Mater.*, 2**003**, 2**,** 413-418.

[121] O. Yosuke, K. Koki, K. Manabu, S. Daizoh, S. T. Shinji, Free-Standing Biodegradable Poly(lactic acid) Nanosheet for Sealing Operations in Surgery, *Adv. Mater.*, **2009**, 43, 4388-4392

[122] R. Ducker, A. Garcia, J. Zhang, T. Chen, S. Zauscher, Polymeric and biomacromolecular brush nanostructures: progress in synthesis, patterning and characterization, *Soft Matter*, **2008**, 4**,** 1774-1786.

[123] R. Jordan, (ed.) Surface-Initiated Polymerization I & II, *Adv. Polym. Sci. vols.* 197&198 (Springer, **2006**).

[124] E. M. Sevick, D. R. M. Williams, Polymer Brushes as Pressure-Sensitive Automated Microvalves, *Macromolecules,* **1994**, 27**,** 5285-5290.

[125] A. Kumar, A. Srivastava, I. Y. Galaev, B. Mattiasson, Smart polymers: physical forms and bioengineering applications, *Prog. Polym. Sci.*, **2007**, 32**,** 1205-1237.

[126] M. Steenackers, R. Jordan, A. Küller, M. Grunze, Engineered Polymer Brushes by Carbon Templating, *Adv. Mater.*, **2009,** 21, 2921-2925.

[127] M. Steenackers, S. Q. Lud, M. Niedermeier, P. Bruno, D. M. Gruen, P. Feulner, M. Stutzmann, J. A. Garrido, R. Jordan, Structured Polymer Grafts on Diamond, *J. Am. Chem. Soc.,* **2007**, 129, 15655-15661.

[127] N. Zhang, M. Steenackers, R. Luxenhofer, R. Jordan, Bottle-Brush Brushes: Cylindrical Molecular Brushes of Poly(2-oxazoline) on Glassy Carbon, *Macromolecules,* **2009**, 42**,** 5345-5351.

[129] J. Genzer, J. Groenewold, Soft matter with hard skin: From skin wrinkles to templating and material characterization, *Soft Matter,* **2006**, 2, 310-323.

[130] J. Groenewold, Wrinkling of plates coupled with soft elastic media, *Physica A*, **2001**, 298, 32-45.

[131] Z. Y. Huang, W. Hong, Z. Suo, Nonlinear analyses of wrinkles in a film bonded to a compliant substrate, *J. Mech. Phys. Solids,* **2005**, 53, 2101-2118.

[132] E. A. Wilder, S. Guo, S. Lin-Gibson, M. J. Fasolka, C.M. Stafford, Measuring the Modulus of Soft Polymer Networks via a Buckling-Based Metrology, *Macromolecules,* **2006**, 39, 4138-4143 (2006).

[133] D. R. M. Williams, Grafted polymers in bad solvents: octopus surface micelles, *J. Phys. II France,* **1993**, 3**,** 1313-1318.

[134] C. Yeung, A. C. Balazs, D. Jasnow, Lateral instabilities in a grafted layer in a poor solvent, *Macromolecules* **1993**, 26**,** 1914-1921.

[135] H. Wang, H. R. Brown, Self-Initiated Photopolymerization and Photografting of Acrylic Monomers, *Macromol. Rapid Commun.*, **2004**, 25**,** 1095-1099.

[136] J. Deng, W. Yang, B. Ranby, FT-IR and Isotherm Study on Anion Adsorption onto Novel Chelating Fibers, *Macromol. Rapid Commun.*, **2001**, 22, 535-539.

[137] S. M. Pimblott, J. A. LaVerne, A. AlbaGarcia, L.D. Siebbeles, Energy Loss by Nonrelativistic Electrons and Positrons in Polymers and Simple Solid Hydrocarbons, *J. Phys. Chem. B,* **2000**, 104, 9607-9614.

[138] J. J. Vlassak, W. D. Nix, A new bulge test technique for the determination of Young's modulus and Poisson's ratio of thin films, *J. Mater. Res.*, **1992**, 7, 3242-3249.

[139] P. Martins, P. Delobelle, C. Malhaire, S. Brida, D. Barbier, Bulge test and AFM point deflection method, two technics for the mechanical characterisation of very low stiffness freestanding films, *Eur. Phy. J. Appl. Phys.*, **2009**, 45, 10501.

[140] J. Bandrup, E. H. Immergut, *Polymer Handbook 3rd ed.* (Wiley, **1989**).

[141] D. Julthongpiput, M. LeMieux, V. V. Tsukruk, Micromechanical properties of glassy and rubbery polymer brush layers as probed by atomic force microscopy, *Polymer*, **2003**, *44*, 4557 4562.

[142] A. Beyer, A. Godt, I. Amin, C. T. Nottbohm, C. Schmidt, J. Zhao, A. Gölzhäuser, Fully cross-linked and chemically patterned self-assembled monolayers, *Phys. Chem. Chem. Phys.*, **2008**, 10, 7233-7238.

Abbreviations

2D (3D) 2 (3) Dimension

4VP 4-vinylpyridine

AA acrylate acid

AFM atomic force microscopy

AIBN N,N-azobisisobutyronitril

ATR-FTIR attenuated total reflectance Fourier transform infrared

ATRP atom transfer radical polymerization

BDE bond dissociation energy

BP benzophenone

BPT 1,1'-biphenyl-4-thiol

cABPT crosslinked 4'-amino-1,1'-biphenyl-4-thiol

cBPT crosslinked BPT

DCM dichloromethane

DMF N,N- dimethylformamide

DP degree of polymerization

DPN dip pen nanolithography

DRIFT diffusion reflectance fourier transformation

EBCD electron beam induced carbon deposition

EBCDs electron beam induced carbon deposits

EBCL electron beam chemical lithography

Eq. equation

ETFE ethylene-co-tetrafluoroethylene

EUV extreme ultraviolet

eV electron volt

Fig. figure

FCCP fully crosslinked and chemically pattern

FWHM full width half maximum

GA glycidyl acrylate

HEA 2-hydroxyethyl acrylate

HEMA 2-hydroxyethyl methacrylate

IR infrared

LBL layer by layer

MAA methacrylic acid

mC micro Coulomb

MEMS microelectromechanical systems

NBPT 4’-nitro-1,1’-biphenyl-4-thiol

NMP nitroxide-mediated polymerization

NMR nuclear magnetic resonance

P4VP poly(4-vinylpyridine)

PDMS poly(dimethyl siloxane)

PE polyethylene

PET poly(ethylene terephthalate)

PMAA poly(methacrylic acid)

PMMA poly(methyl methacrylate)

PP polypropylene

PS polystyrene

PVC polyvinylchloride

RAFT reversible addition-fragmentation chain transfer polymerization

rms root-mean-square

SAM self-assembled monolayer

SEM scanning electron microscope

SIP surface-initiated polymerization

SIPGP self-initiated photografting and photopolymerization

SIPP surface-initiated photopolymerization

SPM scanning probe microscopy

St styrene

STEM scanning transmission electron micrsocopy

STM scanning tunneling microscopy

TEM transmission electrom microscopy

UV ultraviolet

XPS X-ray photoelectron spectroscopy

μCP microcontact printing

List of figures

(I) BPT monolayer obtained by self-assembly on a bare gold surface; (II) after one day of immersion in a solution of NBPT in DMF at 55^{O} C, the BPT SAM is almost completely (~90%) replaced by NBPT; (III) electron irradiation converts the nitro into amino groups.

Figure 5.5 Kinetic of the exchange of NBPT for BPT (process A) and of BPT for NBPT (process B) in DMF at 55 ^{O}C based on XPS data. The nitrogen/carbon-ratio R_{NC} denominates I_{NC} (after exchange) normalized to the value of I_{NC} for a NBPT SAM. Fitting the data with the equations for Langmuir kinetics yields a three-times-higher exchange rate constant km for process A in comparison to process B.

Figure 5.6 (a) AFM image (contact mode) showing the topography of a fully cross-linked, chemically patterned monolayer obtained through process A. The amino terminated areas (inside the circles) appear higher by ~3 Å in comparison to the BPT areas (outside the circles). (b) AFM topography of a fully cross-linked chemically patterned monolayer obtained by process B. For the next step, a surface functionality test on our FCCP monolayers has been performed.

Figure 5.7 AFM images (contact mode) showing the topography of a fully cross-linked and chemically patterned monolayer after treatment with pentanoic acid chloride in the presence of ethyldiisopropylamine. (a) Process A furnishes SAMs with the amino terminated areas inside the circles. (b) Process B resulted in SAMs with the amino terminated areas outside of the circles.

Figure 5.8. Optical microscopy images: (a) Stencil mask used for imposing a pattern into BPT monolayer. This copper grid is coated by a 20 nm thin carbon foil

with micron-sized elliptic and circular openings. (b) A fully cross-linked, chemically patterned monolayer after transfer onto a silicon dioxide surface. The monolayer covers almost the complete millimeter-sized field of view except for a small region on the right side. (c) The pattern within the monolayer becomes visible after a contrast enhancement. The BPT areas (circles and ellipses) have a slightly higher contrast, which indicates an increased refractive index or a higher thickness. This is consistent with the AFM images.

Figure 5.9 AFM images of positive pattern FCCP nanosheet: a) before b) after functionalization with pentanoic acid chloride in the presence of ethyldiisopropylamine in 1,2-dichloroethane solvent.

Figure 5.10 a) Schematic illustration of the preparation of polymer carpets. The electron irradiation of the 4'-nitro-1-1'-biphenyl-4-thiol (NBPT) SAM on gold results in a cross-linked 4'-amino-1,1'-biphenyl-4-thiol (cABPT) SAM. After dissolution of the gold substrate and deposition onto a silicon wafer, a cABPT nanosheet is obtained. Polymer carpets are obtained by SIPGP of a vinyl monomer on the cABPT nanosheet. Optical image of nanosheet (b) before c) after 4hr polymerization of styrene. Both are at the same scale.

Figure 5.11 True to scale 3D representations of AFM measurements of PS carpet edges on silicon. a) UV irradiation time: 0.5h; PS nanocarpet thickness: 19 ± 7 nm. b) UV irradiation time: 16 h. Here, the PS nanocarpet thickness could not be determined accurately by AFM due to the high buckling amplitude (approximately 1.5 µm rms).

Acknowledgements

First of all, I would like to express my very special thanks to *Prof Dr. Armin Gölzhäuser* for opportunity he gave me to do PhD in his research group. His excellent supervision and the possibility he offered me to work on this very exciting topic. I also want to thank him for the patient he shows me during this work and his helpful advices. Dear Prof, it was very tough and very difficult at the beginning. At the end, I am happy I get it through.

I would also like to thank deeply to *Dr. Andre Beyer*, my daily supervisor, for his guidance and patience during this PhD work and his helpful advices.

My deepest thank to Dr. Marin Steenackers, Ning Zhang, and Prof. Dr. Rainer Jordan from the Wacker Lehrstuhl für Makromolekulare Chemie, TU München. The work presented in this thesis is a result of a fruitful collaboration.

Thank to Prof. Adelheid Godt, Christian Schmidt and Daniela Maag from Organic Chemistry Department of Universität Bielefeld for their collaboration and help during my work.

My warmest thank also go to all member of D0 Supramolecular System for their constant helpfulness and for the nice atmosphere I have been enjoying during my stay in Bielefeld. Dr. Berthold Völkel, to whom I always come whenever I need some technical help for my work. Xianghui Zhang with his expertise in mechanical properties measurement which gives contribution to this work. Christoph Nottbohm, Matthias Bünfeld and Mark Schnietz for discussions both

about lab and life outside the lab. Laxman Kankate, with whom I discuss many things, Nils Mellech, Zheng Zhikun, Elina Oberländer, Hening Vieker, Heiko Muzik, Dr. Andrei Turchanin, and Dr. Udo Werner.

Dear Frau Lorentzen, I do not know how to say, but, here is my warmest thank for your kind helps during my stay in Bielefeld. You helped me a lot not only for administration matters, but also for my daily life. Thank you.

My deepest thank to my Indonesian friends. To Ponky Ivo whom I always call almost every night, and ex-berliner Yuni Krisnandi with her ready-to-go traveling style. Specially to Tante Iyu (Yuliani Krisnawati), Tante Nobi (Novi Wibowo), and Eka Sartikawati, for their patience and companion. Cooking and companion are their best in keeping me happy. The Nugrohos (Eko and Kanty Kusmayanty Nugroho) who patiently and continuously provided me with food and films when I went back home from working late in the lab. Dear guys, I do enjoy our time together.

Dr. Hans Doddema for reading my thesis and giving helpful corrections. Dear Hans, thank for all support you have shown me through all the years.

Finally, I would like to thank my parents. Dear father, it has been almost a decade that I am away from home. I am on the way to make my own life now. My talk-active mother, whom I always call every time I feel desperate and stuck in my research. Dear mother, thank you for always encouraging and supporting me for all the years.